KCNN4 links PIEZO-dependent mechanotransduction to NLRP3 inflammasome activation

Li Ran[1,2,3,4#], Tao Ye[1,2,3,4], Eric Erbs[1,2,3,4], Izabela Sumara[1,2,3,4], Romeo Ricci[1,2,3,4,5*] and Zhirong Zhang[1,2,3,4#*]

Affiliations:

[1]Institut de Génétique et de Biologie Moléculaire et Cellulaire, Illkirch, France

[2]Centre National de la Recherche Scientifique, UMR7104, Illkirch, France

[3]Institut National de la Santé et de la Recherche Médicale, U964, Illkirch, France

[4]Université de Strasbourg, Illkirch, France

[5]Laboratoire de Biochimie et de Biologie Moléculaire, Nouvel Hôpital Civil, Strasbourg, France

[#]These authors contributed equally to this work

*Correspondence to: romeo.ricci@igbmc.fr or zhirong.zhang@igbmc.fr

Abstract:

Immune cells sense their microenvironment to fine-tune their inflammatory responses. Patients with cryopyrin associated periodic syndrome (CAPS), caused by mutations in the *NLRP3* gene, present auto-inflammation. However, its manifestation is largely dependent on environmental cues through so far unknown mechanisms. Here, we link PIEZO-mediated mechanotransduction to NLRP3 inflammasome activation. Yoda1, a PIEZO1 agonist, dramatically lowers the threshold for NLRP3 inflammasome activation. PIEZO-mediated stiffness-sensing increases NLRP3-dependent inflammatory responses. Activation of PIEZO1 triggers calcium influx, which activates KCNN4, a calcium-activated potassium channel, to evoke potassium efflux promoting NLRP3 inflammasome activation. Activation of PIEZO1 is sufficient to activate the inflammasome in cells expressing CAPS-causing NLRP3 mutants in a KCNN4-dependent manner. We thus propose that PIEZO-dependent mechanosensing is essential for triggering auto-inflammation in CAPS.

One Sentence Summary: PIEZO-dependent mechanotransduction stimulates KCNN4-dependent potassium efflux to potentiate NLRP3 inflammasome activation.

Main Text:

Immune cells primarily respond to pathogen exposure using pattern recognition receptors (PRRs) to elicit an inflammatory response (*1*, *2*). However, it is increasingly recognized that other parameters in the microenvironment alter in the course of inflammation and that innate immune cells are capable to adapt their responses to those variations. More recently, changes in immune cell activation in response to mechanical cues has been put forward. It has been demonstrated that impaired PIEZO1-dependent mechanosensation in myeloid cells alters their inflammatory response (*3*–*6*). While these studies primarily linked PIEZO1 signaling to transcription of cytokine and chemoattractant, we asked the question whether mechanotransduction has an impact on pattern recognition receptor activation itself. The intracellular NLRP3 inflammasome receptor was one potential candidate given its capacity to detect a remarkable variety of environmental cues (*7*–*10*). Moreover, gain of function mutations in the *NLRP3* gene lead to the development of Cryopyrin-Associated Periodic Syndromes (CAPS), an auto-inflammatory condition that often occurs at joints and eyes, highly mechanical sites, and that can be triggered via cold exposure (*11*).

NLRP3 inflammasome activation requires two principal steps, priming through Toll-like or cytokine receptor signaling resulting in robust expression of the inflammasome components and activation leading to inflammasome complex assembly (*7*–*10*). Assembly includes recruitment of the adaptor protein ASC that binds pro-Caspase-1, leading to self-activation of Caspase-1. Active Caspase-1 cleaves pro-IL-1β and pro-IL-18 into their mature forms promoting their secretion and also cleaves Gasdermin D triggering pro-inflammatory lytic cell death, called pyroptosis (*7*–*10*). We wondered whether PIEZO-mediated mechanotransduction alters NLRP3 inflammasome activation. To this end, we used Yoda1, a PIEZO1 agonist (*12*), and THP-1 cells, a human acute leukemia monocytic cell line widely used for assessing NLRP3 inflammasome activation. THP-1 cells in suspension were primed with LPS and exposed to nigericin to activate the NLRP3 inflammasome in absence or presence of Yoda1. Yoda1 significantly enhanced susceptibility of THP-1 cells to nigericin-induced NLRP3 inflammasome activation as evidenced by increased amounts of cleaved and secreted IL-1β and Caspase-1 in supernatants measured by ELISA and/or Western blotting (Fig. 1, A and 1B) and enhanced pyroptosis determined by Sytox Green uptake (Fig. 1C). Nigericin induces NLRP3 inflammasome activation in a potassium efflux-dependent manner (*13*), we thus wondered if it was the same with potassium efflux-independent activators, imiquimod R837 and its derivative CL097 (*14*). Yoda1 also dramatically lowered the threshold of NLRP3 inflammasome activation in response to R837 or its derivative CL097 (fig. S1, A-F). No induction of pyroptosis was observed in *NLRP3* knockout (KO) THP-1 cells (Fig. 1C and fig. S1C, S1F) confirming that Yoda1-induced potentiation was NLRP3-dependent. The release of cleaved IL-1β and Caspase-1 in response to LPS plus nigericin, R837 or CL097 were also markedly enhanced in Yoda1-stimulated murine bone marrow-derived macrophages (BMDMs) as compared to control-treated cells (fig. S1, G-L). In line with previous study (*4*), Yoda1 treatment also slightly enhanced the production of TNFα, which is not directly linked to inflammasome activation. Formation of ASC specks is a hallmark of cells in which the NLRP3 inflammasome is activated (*15*). LPS-primed BMDMs stimulated with nigericin (Fig. 1D), R837 (fig. S1, M and N) or CL097 (fig. S1, M and N) showed significantly enhanced cell numbers containing ASC specks when co-treated with Yoda1 as compared to cells without Yoda1 treatment. Yoda1 had no such effect on activation of the AIM2-, or pyrin inflammasome (fig. S2, A and B).

To confirm that the effect of Yoda1 on NLRP3 inflammasome activation was PIEZO-dependent, we next generated *PIEZO1* KO, *PIEZO2* KO and *PIEZO1*/2 double knockout (dKO) THP-1 cells using CRISPR/Cas9-mediated gene editing. Deletion of either gene in THP1 cells was confirmed

using Sanger sequencing (fig. S3, A-C). Yoda1-induced potentiation of inflammasome activation in response to nigericin (fig. S4, A-C), R837 (fig. S4, D-F) or CL097 (fig. S4, G-I) was abolished in *PIEZO1* KO and *PIEZO1/2* dKO cells but not in *PIEZO2* KO cells, confirming that effects of Yoda1 occur through PIEZO1 activation. Deletion of both *PIEZO1* and *PIEZO2* did not affect canonical inflammasome activation in response to nigericin, R837 or CL097 in the absence of Yoda1 (fig. S5, A-I). Re-expression of PIEZO1 in *PIEZO1* KO THP-1 cells restored the increased sensitivity to inflammasome activation in response to nigericin (Fig. 1, F-H), R837 (fig. S6, A-C) or CL097 (fig. S6, D-F). We next generated wild type (WT) and *NLRP3* KO THP-1 cells ectopically expressing PIEZO1. In WT cells ectopically expressing PIEZO1, Yoda1 was sufficient to trigger cleavage and secretion of IL-1β and Caspase-1 as well as pyroptosis; while Yoda1 didn't show such effects in *NLRP3* KO cells ectopically expressing PIEZO1 (fig. S7, A-C).

PIEZO1 senses microenvironmental stiffness modulating macrophage function (*3–5*). THP-1 cells cultured on stiff substrates secreted more IL-1β than cells cultured on soft substrates in response to nigericin and R837 (Fig. 1I). Deletion of *PIEZO1* and *PIEZO2* attenuated the secretion of IL-1β triggered by nigericin and R837 in cells cultured on stiff substrates (Fig. 1I). A reduction of secretion of IL-1β was also observed in *PIEZO1/2* dKO cells cultured on soft substrates (Fig. 1I). Our data thus demonstrate that PIEZO1 activation or PIEZO protein-mediated stiffness-sensing lowers the threshold for NLRP3 inflammasome activation.

Activation of PIEZO channels evoke cellular Ca^{2+} influx (*16*). We thus monitored cytosolic Ca^{2+} level using a genetically-encoded fluorescent Ca^{2+} indicator, jGCaMP7S (*17*), in WT and *PIEZO1/2* dKO THP-1 cells treated with R837 in absence or presence of Yoda1. Increase of cytosolic Ca^{2+} levels occurred in presence of Yoda1 in WT cells but not when treated with R837 alone (fig. S8A). In contrast, cells lacking *PEIZO1* and *PIEZO2* did not show obvious increase of cytosolic Ca^{2+} in response to Yoda1 or R837 plus Yoda1 (fig. S8A). We then asked whether potentiation of NLRP3 inflammasome activation by Yoda1 was Ca^{2+} influx-dependent. To this end, we compared the effect of Yoda1 in THP-1 cells treated in culture medium with or without Ca^{2+}. Indeed, enhanced IL-1β and Caspase-1 release and pyroptosis in presence of Yoda1 in R837 and CL097-treated cells were significantly decreased when cells were treated in Ca^{2+}-free medium as compared to cells treated in Ca^{2+}-containing medium (fig. S8, B-G). Thus, Ca^{2+} influx contributes to PIEZO1-mediated potentiation of NLRP3 inflammasome activation.

What is the mechanism by which PIEZO1-mediated Ca^{2+} influx amplifies NLRP3 inflammasome activation? To address this question, we have chosen to perform a genome-wide CRISPR/Cas9-mediated knockout screen in THP-1 cells stably expressing Cas9 using the human CRISPR Brunello lentiviral pooled sgRNA library (*18*). We used R837 to induce NLRP3 inflammasome activation to set up this screen. To obtain hits specifically related to PIEZO1-dependent mechanisms of inflammasome activation, we have chosen a R837 concentration in which co-treatment with R837 and Yoda1 led to approximately 85% cell death, while stimulation with R837 alone resulted in basic level (10 to 15%) of cell death. R837 plus Yoda1-induced cell death was applied twice to ensure maximal elimination of Yoda1-sensitive cells. For the assessment of enrichment of sgRNAs, co-treated cells were compared to vehicle control-treated cells (Fig. 2A). In this screen, NLRP3, ASC (PYCARD) and PIEZO1 were identified as top hits as expected. In addition, ATP11A and CDC50A (TMEM30A), which were reported to directly mediate PIEZO1 activation on membranes (*19*), were also identified. Very intriguingly, KCNN4, a calcium-activated potassium channel which was reported to act downstream of PIEZO1 in red blood cell (*20*), was the first-ranked hit. We further validated the involvement of KCNN4 in this context using both genetical and pharmacological approaches. Deletion of *KCNN4* using CRISPR/Cas9-

mediated gene editing in THP-1 cells (fig. S9) attenuated the enhancing effect of Yoda1 on R837-induced pyroptosis, cleavage and secretion of IL-1β and Caspase-1 (Fig. 2, B-D and fig. S10, A-C). Re-expression of EGFP-tagged KCNN4 restored the enhancing effect of Yoda1 on NLRP3 inflammasome activation in *KCNN4* KO cells (Fig. 2, B-D). In line with previous results obtained in *PIEOZ1/2* dKO cells, deletion of *KCNN4* didn't affect NLRP3 inflammasome activation induced by nigericin, R837 or CL097 alone (fig. S11, A-F). Consistently, pharmacological inhibition of KCNN4 by TRAM-34 (*21*) similarly inhibited pyroptosis, cleavage and secretion of IL-1β and Caspase-1 induced by R837 plus Yoda1 in THP-1 cells (fig. S12, C-E). Similar results were also obtained in BMDMs (fig. S11, F and G). To further consolidate the role of KCNN4-mediated potassium efflux mediating the effect of Yoda1 on NLRP3 inflammasome activation, we blocked potassium efflux by increasing extracellular potassium concentrations and assessed its effect on NLRP3 inflammasome activation. In line with previous studies (*13*, *14*, *22*), increasing extracellular potassium concentrations completely blocked nigericin-induced, but not R837-induced pyroptosis, cleavage and secretion of IL-1β and Caspase-1 (Fig. 2, E-G and fig. S12A, S12B). However, increasing extracellular potassium concentrations completely blocked enhancing effects of Yoda1 on R837-induced NLRP3 inflammasome activation (Fig. 2, E-G and fig. S12, C-G). These results suggest that potassium efflux via KCNN4 mediates the enhancing effect of PIEZO1 activation on NLRP3 inflammasome activation.

In CAPS patients, auto-activation of NLRP3 inflammasome occurs in absence of infection or tissue injury (*11*). However, inflammation occurs at sites of mechanical impact and in response to cold exposure (*11*). We thus asked whether PIEZO-dependent mechanotransduction was important in triggering auto-activation of the NLRP3 inflammasome in CAPS patients. To this end, we expressed three CAPS-causing NLRP3 (mouse) mutants, D301N, T346M and R258W, in *NLRP3*-deficient THP-1 cells. *NLRP3*-deficient cells expressing WT NLRP3 or GFP and WT cells expressing GFP were used as controls. Expression of NLRP3 and GFP was confirmed by Western blotting (fig. S13B). Pyroptotic cell death was determined by propidium iodide incorporation. In line with previous studies (*23–26*), cells expressing CAPS-causing NLRP3 mutants displayed significantly enhanced pyroptosis in response to LPS alone as compared to control-treated cells and LPS-treated control cells (fig. S13A). Importantly, Yoda1 stimulation was sufficient to induce pyroptosis in CAPS-causing NLRP3 mutants expressing cells as compared to control-treated cells (Fig. S13A). Similar to LPS treatment, Yoda1 had only minor effects on induction of pyroptosis in control cells (fig. S13, A and B). We next expressed GFP, WT NLRP3 and CAPS-causing NLRP3 mutants in WT, *PIEZO1* KO, *PIEZO2* KO and *PIEZO1/2* dKO THP-1 cells. The expression of NLRP3 and GFP was confirmed by Western blotting (fig. S13C). LPS-induced pyroptosis in cells expressing CAPS-causing NLRP3 mutants was not dependent on PIEZO1 or PIEZO2 as the response was unaltered in *PIEZO1* KO, *PIEZO2* KO and *PIEZO1/2* dKO cells (fig. S13D). However, Yoda1-induced pyroptosis in cells expressing CAPS-causing NLRP3 mutants depended on PIEZO1 expression (Fig. 3A). We further tested whether PIEZO1-dependent activity was KCNN4-dependent. Indeed, inhibition of KCNN4 dramatically inhibited Yoda1-induced inflammasome activation in these cells (Fig. 3, B and C). Mice carrying the *NLRP3*^{A350V} mutation develop CAPS-like symptoms (*24*). To test whether activation of PIEZO1 is sufficient to activate inflammasome in cells endogenously expressing a CAPS-causing NLRP3 mutant, liver macrophages were isolated from these mice. Cells were primed with low dose of LPS to ensure the expression of NLRP3 and IL-1β and further treated with Yoda1. Low dose of LPS induced moderate secretion of IL-1β as expected (Fig. 3D). Treatment of Yoda1 potentiated secretion of IL-1β, while no IL-1β was detected in control cells under tested conditions (Fig. 3D). Importantly,

inhibition of KCNN4 attenuated Yoda1-induced inflammasome activation in these cells (Fig. 3D). Thus, activation of PIEZO1 by Yoda1 is sufficient to activate the inflammasome in cells expressing CAPS-causing NLRP3 mutants. Altogether, our results suggest that KCNN4 acts downstream of PIEZO1-induced Ca^{2+} influx to promote NLRP3 inflammasome activation, a mechanism that may contribute to environmental effects on severity of CAPS.

Immune cells including macrophages are constantly exposed to microenvironmental changes, such as shear stress in the circulation during extravasation, membrane reorganization during transmigration, hydrostatic pressure in blood vessels, lung and heart (*27*). These changes redirect their responses to physiological and pathological cues (*27*). The NLRP3 inflammasome plays critical roles in innate immune responses detecting various endogenous and exogenous danger signals. In this study, we have provided a direct link between PIEZO protein-mediated mechanosensing and NLRP3 inflammasome-dependent immune response. Activation of PIEZO1 lowers the threshold of NLRP3 inflammasome activation in presence of its activators. However, activation of PIEZO1 by Yoda1 is not sufficient to activate NLRP3 inflammasome in wild type THP-1 cells and BMDMs. However, boosting PIEZO1-signalling by overexpressing PIEZO1 and subsequent Yoda1 treatment was sufficient to activate NLRP3 inflammasome. Persistence of mechanical cues are therefore likely to boost NLRP3-mediated inflammatory response *in vivo*. We identified KCNN4 to act downstream of PIEZO protein-mediated calcium influx and to promote NLRP3 inflammasome. Several studies have shown that intracellular Ca^{2+} signaling is involved in NLRP3 inflammasome activation (*28–30*). But the mechanism underlying remained unclear. KCNN4 represents a valid link between Ca^{2+} signaling and potassium efflux, the latter constituting an established prerequisite in NLRP3 inflammasome activation in response to most stimuli. In CAPS patients, inflammation is often more prominent in eyes, joints and bones, sites harboring movement-associated mechanical properties. Moreover, urticaria seen in CAPS patients is frequently cold-induced. In this study, we discovered that PIEZO1 signaling is sufficient to activate the NLRP3 inflammasome in cells expressing CAPS-causing NLRP3 mutants. Thus, targeting of this pathway may provide a novel therapeutic strategy for treatment of CAPS patients and potentially other NLRP3-related inflammatory diseases.

References:

1. R. Medzhitov, Recognition of microorganisms and activation of the immune response. *Nature*. **449**, 819–826 (2007).

2. S. W. Brubaker, K. S. Bonham, I. Zanoni, J. C. Kagan, Innate immune pattern recognition: a cell biological perspective. *Annu Rev Immunol*. **33**, 257–290 (2015).

3. A. G. Solis, P. Bielecki, H. R. Steach, L. Sharma, C. C. D. Harman, S. Yun, M. R. de Zoete, J. N. Warnock, S. D. F. To, A. G. York, M. Mack, M. A. Schwartz, C. S. Dela Cruz, N. W. Palm, R. Jackson, R. A. Flavell, Mechanosensation of cyclical force by PIEZO1 is essential for innate immunity. *Nature*. **573**, 69–74 (2019).

4. H. Atcha, A. Jairaman, J. R. Holt, V. S. Meli, R. R. Nagalla, P. K. Veerasubramanian, K. T. Brumm, H. E. Lim, S. Othy, M. D. Cahalan, M. M. Pathak, W. F. Liu, Mechanically activated ion channel Piezo1 modulates macrophage polarization and stiffness sensing. *Nat Commun*. **12**, 3256 (2021).

5. J. Geng, Y. Shi, J. Zhang, B. Yang, P. Wang, W. Yuan, H. Zhao, J. Li, F. Qin, L. Hong, C. Xie, X. Deng, Y. Sun, C. Wu, L. Chen, D. Zhou, TLR4 signalling via Piezo1 engages and enhances the macrophage mediated host response during bacterial infection. *Nat Commun*. **12**, 3519 (2021).

6. H. Du, J. M. Bartleson, S. Butenko, V. Alonso, W. F. Liu, D. A. Winer, M. J. Butte, Tuning immunity through tissue mechanotransduction. *Nat Rev Immunol* (2022), doi:10.1038/s41577-022-00761-w.

7. E. Latz, T. S. Xiao, A. Stutz, Activation and regulation of the inflammasomes. *Nat Rev Immunol*. **13**, 397–411 (2013).

8. V. A. K. Rathinam, K. A. Fitzgerald, Inflammasome Complexes: Emerging Mechanisms and Effector Functions. *Cell*. **165**, 792–800 (2016).

9. S. Christgen, T.-D. Kanneganti, Inflammasomes and the fine line between defense and disease. *Curr Opin Immunol*. **62**, 39–44 (2020).

10. P. Broz, V. M. Dixit, Inflammasomes: mechanism of assembly, regulation and signalling. *Nat Rev Immunol*. **16**, 407–420 (2016).

11. L. M. Booshehri, H. M. Hoffman, CAPS and NLRP3. *J Clin Immunol*. **39**, 277–286 (2019).

12. R. Syeda, J. Xu, A. E. Dubin, B. Coste, J. Mathur, T. Huynh, J. Matzen, J. Lao, D. C. Tully, I. H. Engels, H. M. Petrassi, A. M. Schumacher, M. Montal, M. Bandell, A. Patapoutian, Chemical activation of the mechanotransduction channel Piezo1. *Elife*. **4** (2015), doi:10.7554/eLife.07369.

13. R. Muñoz-Planillo, P. Kuffa, G. Martínez-Colón, B. L. Smith, T. M. Rajendiran, G. Núñez, K^+ efflux is the common trigger of NLRP3 inflammasome activation by bacterial toxins and particulate matter. *Immunity*. **38**, 1142–1153 (2013).

14. C. J. Groß, R. Mishra, K. S. Schneider, G. Médard, J. Wettmarshausen, D. C. Dittlein, H. Shi, O. Gorka, P.-A. Koenig, S. Fromm, G. Magnani, T. Ćiković, L. Hartjes, J. Smollich, A. A. B. Robertson, M. A. Cooper, M. Schmidt-Supprian, M. Schuster, K. Schroder, P. Broz, C. Traidl-Hoffmann, B. Beutler, B. Kuster, J. Ruland, S. Schneider, F. Perocchi, O. Groß, K+ Efflux-Independent NLRP3 Inflammasome Activation by Small Molecules Targeting Mitochondria. *Immunity*. **45**, 761–773 (2016).

15. A. Stutz, G. L. Horvath, B. G. Monks, E. Latz, ASC speck formation as a readout for inflammasome activation. *Methods Mol Biol*. **1040**, 91–101 (2013).

16. B. Coste, J. Mathur, M. Schmidt, T. J. Earley, S. Ranade, M. J. Petrus, A. E. Dubin, A. Patapoutian, Piezo1 and Piezo2 are essential components of distinct mechanically activated cation channels. *Science*. **330**, 55–60 (2010).

17. H. Dana, Y. Sun, B. Mohar, B. K. Hulse, A. M. Kerlin, J. P. Hasseman, G. Tsegaye, A. Tsang, A. Wong, R. Patel, J. J. Macklin, Y. Chen, A. Konnerth, V. Jayaraman, L. L.

Looger, E. R. Schreiter, K. Svoboda, D. S. Kim, High-performance calcium sensors for imaging activity in neuronal populations and microcompartments. *Nat Methods*. **16**, 649–657 (2019).

18. J. G. Doench, N. Fusi, M. Sullender, M. Hegde, E. W. Vaimberg, K. F. Donovan, I. Smith, Z. Tothova, C. Wilen, R. Orchard, H. W. Virgin, J. Listgarten, D. E. Root, Optimized sgRNA design to maximize activity and minimize off-target effects of CRISPR-Cas9. *Nat Biotechnol*. **34**, 184–191 (2016).

19. M. Tsuchiya, Y. Hara, M. Okuda, K. Itoh, R. Nishioka, A. Shiomi, K. Nagao, M. Mori, Y. Mori, J. Ikenouchi, R. Suzuki, M. Tanaka, T. Ohwada, J. Aoki, M. Kanagawa, T. Toda, Y. Nagata, R. Matsuda, Y. Takayama, M. Tominaga, M. Umeda, Cell surface flip-flop of phosphatidylserine is critical for PIEZO1-mediated myotube formation. *Nat Commun*. **9**, 2049 (2018).

20. S. M. Cahalan, V. Lukacs, S. S. Ranade, S. Chien, M. Bandell, A. Patapoutian, Piezo1 links mechanical forces to red blood cell volume. *Elife*. **4** (2015), doi:10.7554/eLife.07370.

21. H. Wulff, M. J. Miller, W. Hansel, S. Grissmer, M. D. Cahalan, K. G. Chandy, Design of a potent and selective inhibitor of the intermediate-conductance Ca2+-activated K+ channel, IKCa1: a potential immunosuppressant. *Proc Natl Acad Sci U S A*. **97**, 8151–8156 (2000).

22. V. Pétrilli, S. Papin, C. Dostert, A. Mayor, F. Martinon, J. Tschopp, Activation of the NALP3 inflammasome is triggered by low intracellular potassium concentration. *Cell Death Differ*. **14**, 1583–1589 (2007).

23. I. Aksentijevich, C. D. Putnam, E. F. Remmers, J. L. Mueller, J. Le, R. D. Kolodner, Z. Moak, M. Chuang, F. Austin, R. Goldbach-Mansky, H. M. Hoffman, D. L. Kastner, The clinical continuum of cryopyrinopathies: novel CIAS1 mutations in North American patients and a new cryopyrin model. *Arthritis Rheum*. **56**, 1273–1285 (2007).

24. S. D. Brydges, J. L. Mueller, M. D. McGeough, C. A. Pena, A. Misaghi, C. Gandhi, C. D. Putnam, D. L. Boyle, G. S. Firestein, A. A. Horner, P. Soroosh, W. T. Watford, J. J. O'Shea, D. L. Kastner, H. M. Hoffman, Inflammasome-mediated disease animal models reveal roles for innate but not adaptive immunity. *Immunity*. **30**, 875–887 (2009).

25. Y. Nakamura, L. Franchi, N. Kambe, G. Meng, W. Strober, G. Núñez, Critical role for mast cells in interleukin-1β-driven skin inflammation associated with an activating mutation in the nlrp3 protein. *Immunity*. **37**, 85–95 (2012).

26. Z. Zhang, G. Meszaros, W.-T. He, Y. Xu, H. de Fatima Magliarelli, L. Mailly, M. Mihlan, Y. Liu, M. Puig Gámez, A. Goginashvili, A. Pasquier, O. Bielska, B. Neven, P. Quartier, R. Aebersold, T. F. Baumert, P. Georgel, J. Han, R. Ricci, Protein kinase D at the Golgi controls NLRP3 inflammasome activation. *J Exp Med*. **214**, 2671–2693 (2017).

27. M. Huse, Mechanical forces in the immune system. *Nat Rev Immunol*. **17**, 679–690 (2017).

28. G.-S. Lee, N. Subramanian, A. I. Kim, I. Aksentijevich, R. Goldbach-Mansky, D. B. Sacks, R. N. Germain, D. L. Kastner, J. J. Chae, The calcium-sensing receptor regulates the NLRP3 inflammasome through Ca2+ and cAMP. *Nature*. **492**, 123–127 (2012).

29. M. Rossol, M. Pierer, N. Raulien, D. Quandt, U. Meusch, K. Rothe, K. Schubert, T. Schöneberg, M. Schaefer, U. Krügel, S. Smajilovic, H. Bräuner-Osborne, C. Baerwald, U. Wagner, Extracellular Ca2+ is a danger signal activating the NLRP3 inflammasome through G protein-coupled calcium sensing receptors. *Nat Commun*. **3**, 1329 (2012).

30. T. Murakami, J. Ockinger, J. Yu, V. Byles, A. McColl, A. M. Hofer, T. Horng, Critical role for calcium mobilization in activation of the NLRP3 inflammasome. *Proc Natl Acad Sci U S A*. **109**, 11282–11287 (2012).

Acknowledgments: We thank all the membranes in Ricci's laboratory for scientific inputs. We also thank the facilities at IGBMC, including cell cytometry facility, cell culture facility, imaging facility and animal facility, for their technique help during the whole study.

Funding: Work in the laboratory of R.R. was supported by the Agence Nationale de la Recherche (ANR) (AAPG 2017 LYSODIABETES), by the USIAS fellowship grant 2017 of the University of Strasbourg, by the Fondation de Recherche Médicale (FRM) - Program: Equipe FRM (EQU201903007859, Prix Roger PROPICE pour la recherche sur le cancer du pancréas) and by the ANR-10-LABX-0030-INRT grant as well as the ANR-11-INBS-0009-INGESTEM grant, both French State funds managed by the ANR under the frame program Investissements d'Avenir; L.R. was supported by the China Scholarship Council (CSC).

Author contributions: Conceptualization, Z.Z. and R.R.; Methodology, Z.Z., L.R. and T.Y.; Investigation, Z.Z. and L.R.; Writing – Review & Editing, R.R., Z.Z. and L.R.; Funding Acquisition, R.R.; Resources, Z.Z., L.R. and E.E.; Supervision, Z.Z. and R.R..

Competing interests: Authors declare no competing interests.

Data and materials availability: All data is available in the main text or the supplementary materials.

Supplementary Materials:

Materials and Methods

Figures S1-S13

Materials and Methods

Mice

Nlrp3^{A350VneoR} mice were obtained from The Jackson Laboratory and crossed with *LysM-Cre* mice to obtain mice with myeloid-specific expression of NLRP3^{A350V}. Mice were housed under specific pathogen-free conditions with controlled temperature (19-23°C) and humidity (50-60%) on a 12-h light/dark cycle with unrestricted access to water and standard laboratory chow. Maintenance and animal experimentation were in accordance with the local ethical committee (Com'Eth) in compliance with the European legislation on care and use of laboratory animals (La cellule AFiS (Animaux utilisés à des Fins Scientifiques): APAFIS#36729-2022041911158105 v2). No exclusion of animals used for experiments was performed. Littermates were chosen randomly according to their genotypes.

Reagents

Imiquimod (R837) (tlrl-imq), CL097 (tlrl-c97) and MCC950 (inh-mcc) were purchased from InvivoGen. Nigericin sodium salt (N7143), Propidium Iodide (P4170), Lipopolysaccharides from Escherichia coli 055: B5 (L2880) and Phorbol 12-myristate 13-acetate (PMA) (P1585) were obtained from Sigma-Aldrich. Yoda1 (5586) and TRAM34 (2946) were purchased from Bio-techne. Sytox™ Green Nucleic Acid Stain (S7020) was purchased from Thermo Fisher Scientific. Human macrophage-colony stimulating factor (hM-CSF) (11343117) was obtained from Immunotools. Anti-Caspase1 (p20) (human) antibody (AG-20B-0048-C100), anti-Caspase1 (p20) (mouse) antibody (AG-20B-0042), anti-NLRP3 antibody (AG-20B-0014-C100) were purchased from AdipoGen. Anti-human IL-1β antibody (AF-201-NA) was from R&D Systems. Anti-murine IL-1β antibody (5129-100) was from BioVision. Anti-tubulin (T5168) was from Sigma-Aldrich.

Anti-GFP antibody (ab13970) was obtained from Abcam. Anti-ASC antibody (sc-22514) was obtained from Santa Cruz Biotechnology.

Plasmids

The pX330-P2A-EGFP and pX330-P2A-RFP plasmid was previously generated by inserting P2A-GFP and P2A-RFP sequence into pX330-U6-Chimeric_BB-CBh-hSpCas9 (*26*). KCNN4 CDS was amplified from THP-1 cDNA by PCR. KCNN4 fused with EGFP was cloned into pBOB plasmid using ligation-independent cloning (LIC). Calcium reporter jGCaMP7s sequence was amplified from pGP-CMV-jGCaMP7s (104463, Addgene) and cloned into pBOB plasmid by LIC. C-terminal EGFP-tagged CAPS-causing mouse Nlrp3 mutants R258W, D301N and T346M were cloned into pBOB plasmid by LIC. Mouse Piezo1 CDS was amplified from a gift plasmid from Prof. Ardem Patapoutian and cloned into pBOB plasmid by LIC. The primers used are listed below:

Name	**Sequences**
pBOB mPiezo1 CDS-F	5'ATGGAGCCGCACGTGCTGGGCGCCGGGC3'
pBOB mPiezo1 CDS-R	5'CTACTCCCTCTCACGTGTCCACTTA 3'
PBOB KCNN4-EGFP F1	5'ATGGGCGGGGATCTGGTGCTTGGC 3'
PBOB KCNN4-EGFP R1	5'TCCTCGCCCTTGCTCACCATCTTGGACTGCTGGC TGGGTTCTGGA 3'
PBOB KCNN4-EGFP F2	5'AACCCAGCCAGCAGTCCAAGATGGTGAGCAAGG GCGAGGAGCTGT 3'
PBOB KCNN4-EGFP R2	5'CTACTTGTACAGCTCGTCCATGCCG 3'
pBOB-jGCaMP7s-F	5'ATGGGTTCTCATCATCATCATCATC 3'
pBOB-jGCaMP7s-R	5'TTACTTCGCTGTCATCATTTGTACA 3'
mNlrp3 R258W-F	5'TATCCACTGCTGGGAGGTGAGCCTC 3'
mNlrp3 R258W-R	5'GAGGCTCACCTCCCAGCAGTGGATA 3'
mNlrp3 D301N-F	5'TGGATGGCTTTAATGAGCTACAAGG 3'
mNlrp3 D301N-R	5'CCTTGTAGCTCATTAAAGCCATCCA 3'
mNlrp3 T346M-F	5'CTGCTCATAACGATGAGGCCGGTAG 3'
mNlrp3 T346M-R	5'CTACCGGCCTCATCGTTATGAGCAG 3'

Generation of knockout cell lines using CRISPR/Cas9-mediated gene editing

For the generation of *PIEZO1* KO, *PIEZO2* KO, *PIEZO1/2* double knockout (dKO) and *KCNN4* KO THP-1 cell lines, two sgRNAs (sgRNA 1 and sgRNA 2) for each gene were designed and cloned into pX330-P2A-EGFP or pX330-P2A-RFP, respectively, using T4 ligation. THP-1 cells were transfected with mixture of two sgRNAs-expressing plasmids (0.5 μg each) using X-tremeGENE 9 according to the manufacturer's manual. 24 h after transfection, GFP and RFP double-positive cells were sorted and collected using BD FACS Aria™ III Cell Sorter. Single cell colonies were obtained by seeding into 96-well plates via series of dilution. The sequences of sgRNAs are listed below:

Name	**Sequences**
hPIEZO1 sgRNA 1	5' CACCAAGATGCCCAGGTCAG 3'
hPIEZO1 sgRNA 2	5' CCCGGCAGAGCCCACATCCA 3'
hPEZIO2 sgRNA 1	5' TATGAAGAGGATTTCAATGG 3'
hPIEZO2 sgRNA 2	5' AACAACGACTTTCCCAGCAG 3'
hKCNN4 sgRNA 1	5' TTCGGCGTCTCAAGGCCCCC 3'
hKCNN4 sgRNA 2	5' CAGAGATGCTGTGGTTCGGG 3'

Validation of obtained THP-1 knockout cell lines by Sanger sequencing

For the validation of *PIEZO1* KO, *PIEZO2* KO, *PIEZO1/2* dKO, *KCNN4* KO THP-1 clones, genomic fragments containing sgRNA targeting sites were amplified by PCR and cloned into pUC57 plasmid using LIC. After transformation of *E.coli* competent cells, plasmids were purified from at least 6 bacteria colonies and subjected to Sanger sequencing. Obtained sequences were aligned to reference sequence to determine the insertion/deletion. The primers used are listed below:

Name	**Sequences**
PIEZO1 KO GT-F	5' CCTGTCCTCTTGGTCTGACCGCGGC 3'
PIEZO1 KO GT-R	5' CCATGTCGGGGCGTGGAGGTTTCTG 3'
PIEZO2 KO GT-F	5' CTGGTTGTCTTCCCTTTTTTCCTGA 3'
PIEZO2 KO GT-R	5' AACCTAGAAAATGGAGTCGCTTAGC 3'

KCNN4 KO GT-F	5' TGCCCCAAGACACACCCTAGCCCCT 3'
KCNN4 KO GT-R	5' CAAGTCCCCAGTCCCTCCTCCCTCA 3'

Cell culture

THP-1, mouse primary bone marrow-derived macrophages (BMDMs) and HEK293t cell lines were cultured at 37°C with 5% CO2. THP-1 cells were grown in RPMI 1640 supplement with 10 mM HEPES, 10% fetal calf serum (FCS), 2.5 g/l glucose, 1 mM sodium pyruvate, gentamycin and 50 μM β-mercaptoethanol. HEK293t cells were grown in DMEM (1 g/ml glucose) supplement with 10% fetal calf serum, penicillin and streptomycin. BMDMs were differentiated from bone marrow progenitors isolated from the tibia and femur in DMEM (4,5g/l glucose) supplement with 50 ng/ml recombinant hM-CSF, 10% heat-inactivated fetal calf serum, penicillin and streptomycin for 7 days. For treatment of cells, BMDMs and THP-1 cells were primed with 1 μg/mL LPS for 3 h, followed by the treatment of nigericin, Imiquimod and CL097 in presence or absence of 25 μM Yoda1. For treatment of inhibitor, cells were pretreated with inhibitor for 45 min and followed by stimulation in presence of inhibitor. To assess the involvement of K^+ efflux, LPS-primed cells were treated with NLRP3 inflammasome activator in the culture medium supplemented with 5 mM, 15 mM, 25 mM, or 35 mM KCl. For the experiments with calcium-free medium, BMDMs and THP-1 cells were primed with 1 μg/mL LPS for 3h in DMEM (4,5g/l glucose) containing 10% FCS, cells were washed once with PBS before treatment with nigericin, R837 or CL097 in DMEM (4,5g/l glucose) without calcium containing 10% dialyzed FCS. For the stiffness-related experiments, cells seeded on silicone gels of 0.2 Kpa and 64 Kpa (5165-5EA and 5145-5EA, Sigma-Aldrich) with culture medium containing 100 nM PMA for 3 h, followed by replacement of fresh medium and incubation at 37 ℃ overnight. On the next day, cells were treated with nigericin or R837.

Immunoblotting

Both cell lysates and culture supernatants were subjected to immunoblotting. For cell lysates, cells were lysed on ice with 1× RIPA buffer (50 mM Tris-HCl pH 7.5, 150 mM NaCl, 1 mM EDTA, 1 mM EGTA, 1% Triton X-100, 1 mM NaVO4, 1.5 mM Sodium pyrophosphate, 1 mM NaF, 1 mM β-Glycerophosphate) supplemented with protease inhibitor cocktail. The immunoblot was prepared using Glycine SDS-PAGE gels. For the supernatants, the proteins were extracted using methanol-chloroform precipitation protocol as previously described *(26)*, separated by Tricine SDS-PAGE and analyzed by immunoblotting. The PVDF membranes were incubated with primary antibody at 4 °C overnight. After 3 times washes with TBS-T, membranes were incubated with HRP-conjugated secondary antibody for 1 hour at RT. Membranes were again washed with TBS-T for 3 times and were incubated with Immobilon Forte Western HRP substrate (WBLUF0500, EMD Millipore Corporation). Images were captured using AI600 Imager from GE Healthcare Life Science.

Flow cytometry

For analysis of lytic cell death, after treatments, THP-1 cells were spin down and resuspended in cold PBS with 1 μM of Sytox Green or propidium iodide (PI). Sytox Green- or PI- positive cells were analyzed by BD FACS Celesta™ Flow Cytometer. For cell sorting, THP-1 cells were spin down and resuspended in cold PBS supplemented with 1% of fetal calf serum, followed by sorting at sterile condition using BD FACS Aria™ III Cell Sorter in fresh medium for further culture.

Measurement cytokines using ELISA

IL-1β and TNFα levels in collected culture supernatants were determined by ELISA according to the user's manual. Human IL-1 beta/IL-1F2 DuoSet ELISA (DY201), mouse IL-1 beta/IL-1F2 DuoSet ELISA (DY401), human TNF-alpha DuoSet ELISA (DY210), mouse TNF-alpha DuoSet

ELISA (DY410) and DuoSet ELISA Ancillary Reagent Kit 2 (DY008) were purchased from R&D system.

Immunofluorescence and live-video imaging

For immunofluorescence, cells plated on coverslips (12-mm) were fixed with 4% paraformaldehyde for 15 min at room temperature after treatments. Coverslips were washed three times with PBS for 5 min each time and permeabilized with 0.1% saponin in PBS for 10 min, followed by blocking in PBST (PBS plus 0.05% Tween-20) containing 0.5% BSA for 1 h. The coverslips were further incubated with anti-ASC antibody (1/100 dilution) for 1 h at room temperature, followed by incubation with the secondary for 1h at room temperature (avoid the coverslips in direct light). After three times washing with PBST, cells were stained with DAPI and mounted for further imaging. For live-video imaging, THP-1 WT and *PIEZO1/2* dKO cells stably expressing jGCaMP7S were seeded on µ-dish 35 mm high glass bottom (81158, Ibidi) in culture medium containing 100 nM PMA for 3 h, followed by replacement of fresh medium and incubation overnight. On the next day, cells were treated with R837, Yoda1 or R837 plus Yoda1. The images were acquired using a Nikon spinning disk with an interval of 20s. Ionomycin was added at ~16 min after treatment. Fluorescence intensities of individual cells over time were quantified with Image J.

Lentivirus packaging and infection

The 3rd generation lentiviral vector system with three packaging helper plasmids (pVSVG, pMDL and pREV) was used in this study. The lentivirus packaging was performed in HEK293t cells. HEK293t cells were transfected with Lipofectamine 2000 according to the user's manual. THP-1 cells (4.0×10^5 cells per well in 6-well plate) were infected in 1.5 mL lentivirus-contained culture

medium plus 1 mL fresh medium containing final concentration of 10 μg/mL polybrene. 48 hours after viral infection, cells were used for further experiments.

Genome-wide CRISPR/Cas9-mediated knockout screen

The Brunello human genome-wide CRISPR/Cas9 knockout lentiviral library containing 76,441 sgRNAs systemically targeting 19,114 genes on human genome was used in this study. Briefly, THP-1 cells stably expressing Cas9 protein were infected with the pooled Brunello lentivirus library at ROI of 0.2. After puromycin selection for 3 days, cells were further expanded. To ensure a representation of minimal 500 cells per sgRNA, at least 4.0×10^7 cells were used in each group. An adequate number of cells were primed with LPS in suspension for 3 hours and treated with vehicle (control group) or R837 plus Yoda1 (treated group). When pyroptotic cell death reached ~85% in the treated group, R837 and Yoda1 were washed out and the survivals were expanded. When cell number reached 4.0×10^7 cells, these cells were repeatedly treated with R837 plus Yoda1 to reach reached ~85% of pyroptotic cell death. R837 and Yoda1 were washed out and the survivals were further expanded to reach 4.0×10^7 cells. Genomic DNA from both control- and treated groups was isolated using the phenol/chloroform extraction method. Fragments containing sgRNA were amplified from genomic DNA by PCR referring to the protocol from broad institute GPP Web Protal (https://portals.broadinstitute.org/gpp/public/resources/protocols). PCR fragments were cleaned up using NucleoSpin gel and PCR clean-up kit (740609.50, MACHEREY-NAGEL) according to the users' manual and subjected to next generation sequencing (NGS). Sequencing was performed on an Illumina HiSeq 4000 sequencer as 50 bp single end reads by the GenomEast platform, a member of the 'France Genomique' consortium (ANR-10-INBS-0009). Image analysis and base calling were performed using RTA version 2.7.7 and bcl2fastq version 2.20.0.422. Sequencing reads were trimmed, aligned and counted using PinAPL-Py and guide

RNAs (Brunello library). The Matching Threshold for bowtie2 alignment was defined as 35. Data were statistically analyzed using Model-based Analysis of Genome-wide CRISPR/Cas9 Knockout (MAGeCK v0.5.9.3). The method ranks sgRNAs based on *p*-values calculated from the negative binomial model, and uses a modified robust ranking aggregation (RRA) algorithm to identify positively or negatively selected genes. Read counts were normalized by total number of reads. Enrichment testing of paired samples was performed using the test function in MAGeCK with --paired option. Volcano plot was generated using ggplot package in R and significance was defined as FDR < 0.05.

Statistical analysis

Preliminary experiments were performed and sample size was determined based on generally accepted rules to test preliminary conclusions reaching statistical significance, where applicable. For FACS experiments, the percentage of Sytox green-positive and PI-positive cells was provided. For immunofluorescence experiments, a minimum of 150 cells were counted per condition, and the percentage containing ASC specks cells was calculated. Values are presented by “Mean +/- SD”. Unless specified, statistical analyses were performed with the two tailed *t*-test using Prism (GraphPad Software). Statistical significance was indicated using the following symbols: * $p < 0.05$, ** $p < 0.01$ and *** $p < 0.001$.

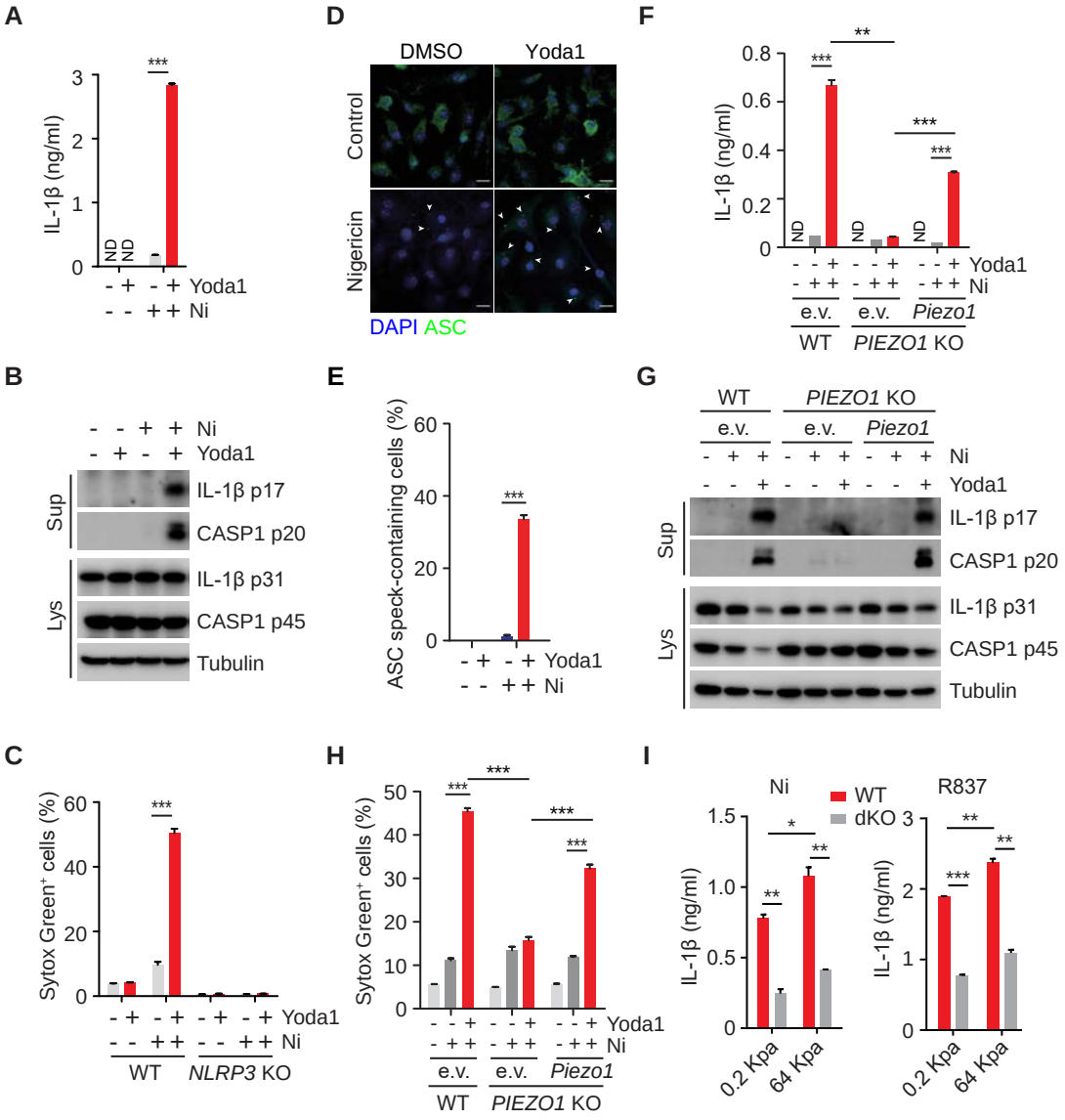

Fig. 1. The PIEZO-mediated mechano-sensing potentiates NLRP3 inflammasome activation. (**A**) ELISA measurements of IL-1β in culture supernatants from THP-1 primed with 1 μg/ml LPS for 3 h and followed by treatment with 5 μM nigericin (Ni) in presence or absence of Yoda1 25 μM. (**B**) Immunoblotting of culture supernatants (Sup) and lysates (Lys) from LPS-primed THP-1 treated as in panel A. Antibodies against IL-1β and Caspase-1 (CASP1) were used. An antibody against Tubulin was used as a loading control. (**C**) Uptake of Sytox Green in LPS-primed wild type (WT) and *NLRP3* KO THP-1 cells treated as described in panel A. (**D**) Representative immunofluorescence images of ASC speck formation in LPS-primed BMDMs stimulated with 2.5 μM nigericin in the presence or absence of 25 μM Yoda1. White arrows indicate ASC specks (green). Scale bars: 10 μm. (**E**) Quantification of macrophages containing ASC specks in experiments as described in panel D. (**F**) ELISA measurements of IL-1β in culture supernatants from WT and *PIEZO1* KO THP-1 cells expressing empty vector (e.v.) or mouse Piezo1. Cells primed with 1 μg/ml LPS for 3 h and followed by treatment with 5 μM nigericin (Ni) in presence or absence of Yoda1 25 μM for 40 min. (**G**) Immunoblotting of culture supernatants (Sup) and lysates (Lys) from LPS-primed cells treated as described in panel F. Antibodies against IL-1β and Caspase-1 (CASP1) were used. An antibody against Tubulin was used as a loading control. (**H**) Uptake of Sytox Green from LPS-primed cells treated as described in panel F. Sytox Green uptake was analyzed by FACS after staining. (**I**) ELISA measurements of IL-1β in culture supernatants from WT and *PIEZO1/2* dKO (dKO) THP-1 cells cultured on soft (0.2 Kpa) or stiff (64 Kpa) silicone. Cells were treated with nigericin (Ni) for 40 min or R837 for 2 h. "ND" not detected. **p* < *0.05*, ***p* < *0.01*, ****p* < *0.001*. Data are representative of at least three independent experiments.

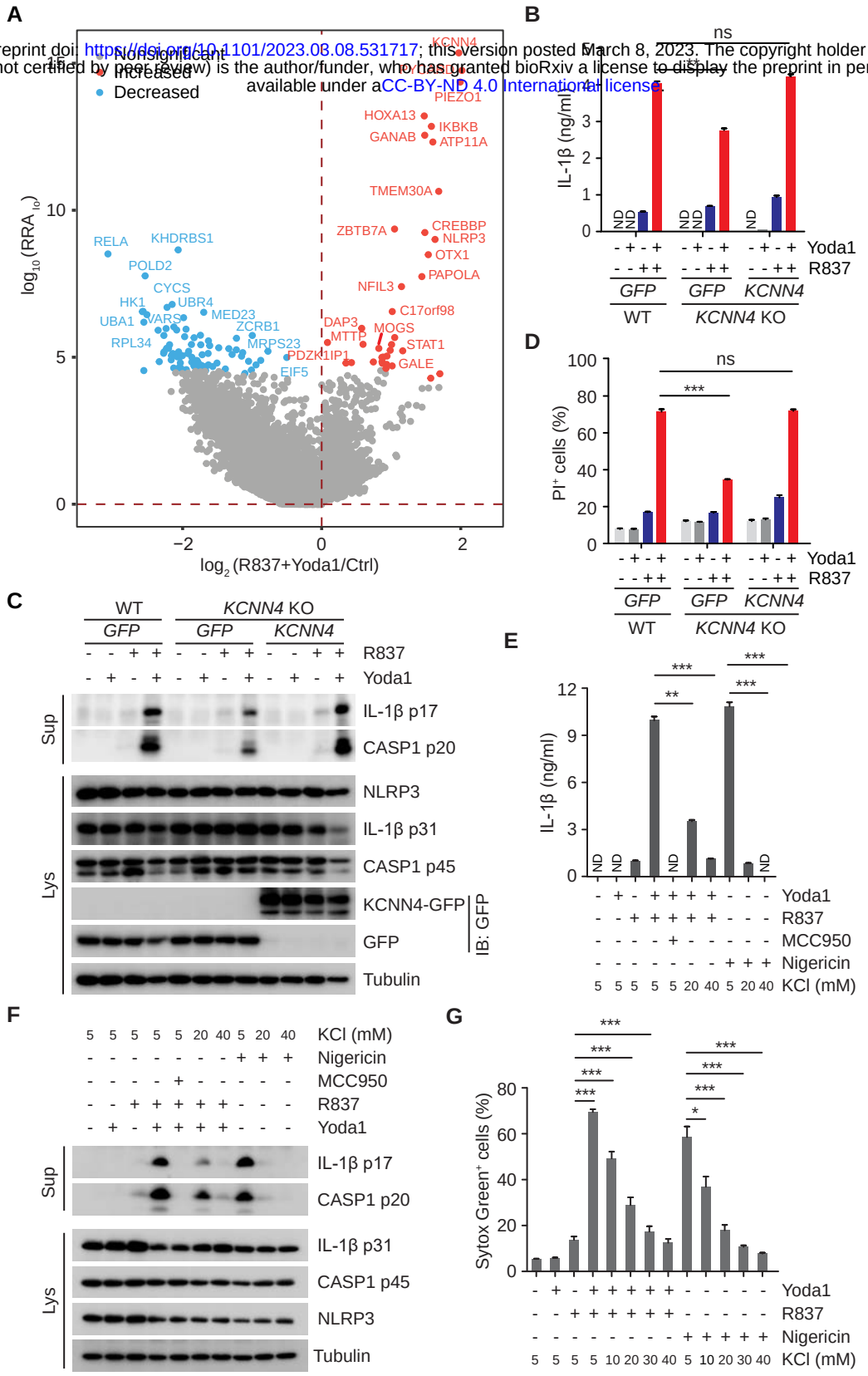

Fig. 2. KCNN4 acts downstream of PIEZO-mediated calcium influx to promote NLRP3 inflammasome activation. (**A**) Genome-wide CRISPR/Cas9 screening identifies genes involved in Yoda1-mediated pyroptosis. RRA score in the comparison R837 plus Yoda1 vs vehicle. (**B**) ELISA measurements of IL-1β in culture supernatants from WT and *KCNN4* KO THP-1 cells expressing GFP or GFP-tagged KCNN4 (KCNN4). Cells primed with 1 μg/ml LPS for 3 h and followed by treatment with 100 μM R837 in presence or absence of Yoda1 25 μM for 1 h. (**C**) Immunoblotting of culture supernatants (Sup) and lysates (Lys) from cells in experiments as described in panel B. Antibodies against IL-1β and Caspase-1 (CASP1) were used. An antibody against Tubulin was used as a loading control. (**D**) Uptake of Propidium Iodide (PI) in LPS-primed cells in experiments as described in panel B. (**E**) ELISA measurements of IL-1β in culture supernatants from LPS-primed BMDMs treated with 50 μM R837 or 15 μM nigericin with or without Yoda1 in medium containing indicated concentration of extracellular KCl. (**F**) Immunoblotting of culture supernatants (Sup) and lysates (Lys) from LPS-primed BMDMs in experiments as described in panel E. (**G**) Uptake of Sytox Green in LPS-primed THP-1 cells followed by treatment of 100 μM R837 or 15 μM nigericin with or without 25 μM Yoda1 in medium containing different concentrations of extracellular KCl. "ND" not detected. "ns" not significant, *$p < 0.05$, **$p < 0.01$, ***$p < 0.001$. Data are representative of at least three independent experiments.

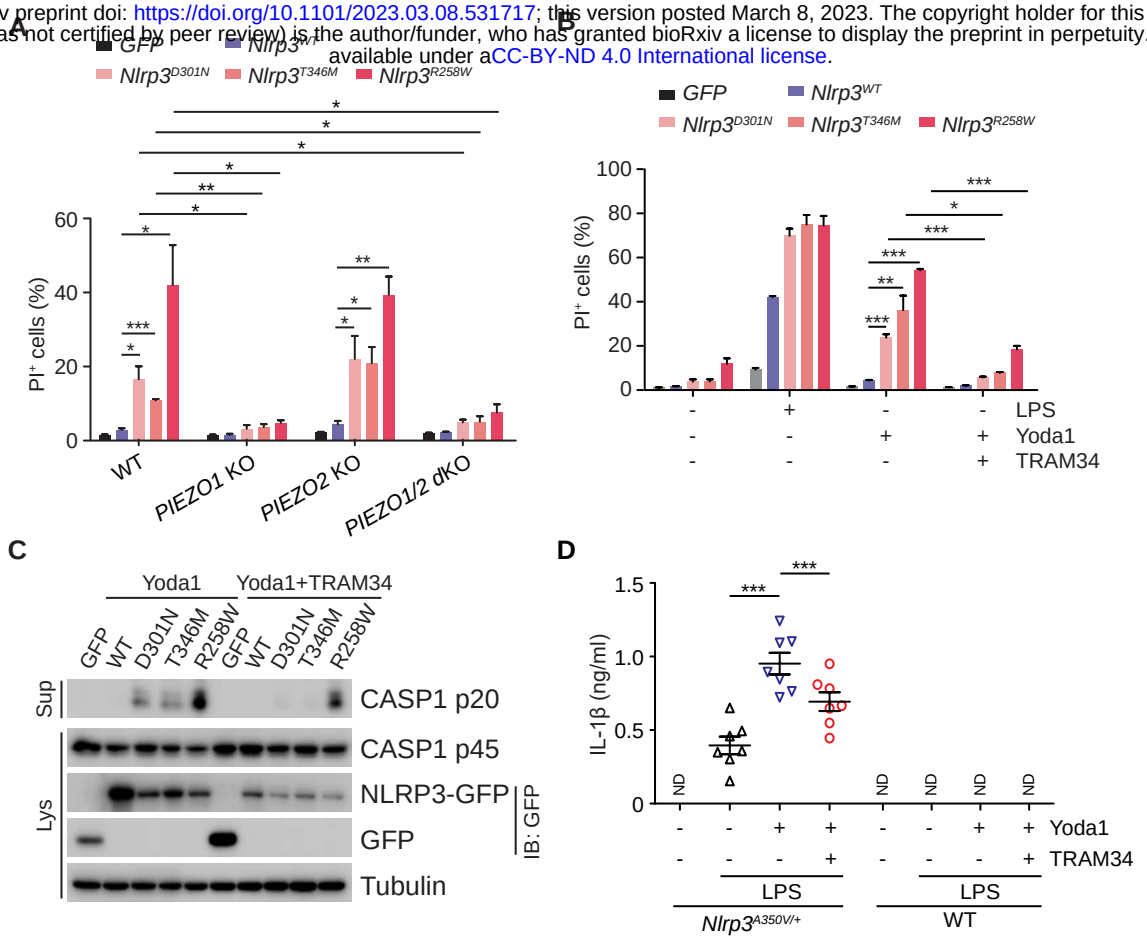

Fig. 3. Actication of PIEZO1 is sufficient to trigger NLRP3 inflammasome activation in cells expressing CAPS-causing NLRP3 mutants. (**A**) Uptake of Propidium Iodide (PI) in WT, *PIEZO1* KO, *PIEZO2* KO and *PIEZO1/2* dKO THP-1 cells expressing GFP, WT- or D301N-, T346M-, R258W mutated mouse Nlrp3. Cells were treated with 25 μM Yoda1 for 6 h. (**B**) Uptake of Propidium Iodide (PI) in WT THP-1 cells expressing GFP, WT- or D301N-, T346M-, R258W mutated mouse Nlrp3. Cells were treated with vehicle, 1 μg/ml LPS, 25 μM Yoda1 or 25 μM Yoda1 plus 5 μM TRAM34 for 6h. (**C**) Immunoblotting of culture supernatants (Sup) and lysate(Lys) from WT THP-1 cells expressing GFP, WT- or D301N-, T346M-, R258W mutated mouse Nlrp3. Cells were treated with 25 μM Yoda1 in presence or absence of 5 μM TRAM34 for 6h. Antibodies against Caspase-1 (CASP1) and GFP were used. An antibody against Tubulin was used as a loading control. (**D**) ELISA measurements of IL-1β in culture supernatants in fetal liver macrophages from mice (n=7) as indicated. Cells were primed with 1 ng/ml LPS for 1 h, followed by treatment with vehicle or 25 μM Yoda1 in presense or absence of 5 μM TRAM34 for 3 h. "ND" means not detected. *$p < 0.05$, **$p < 0.01$, ***$p < 0.001$. Data are representative of at least three independent experiments.

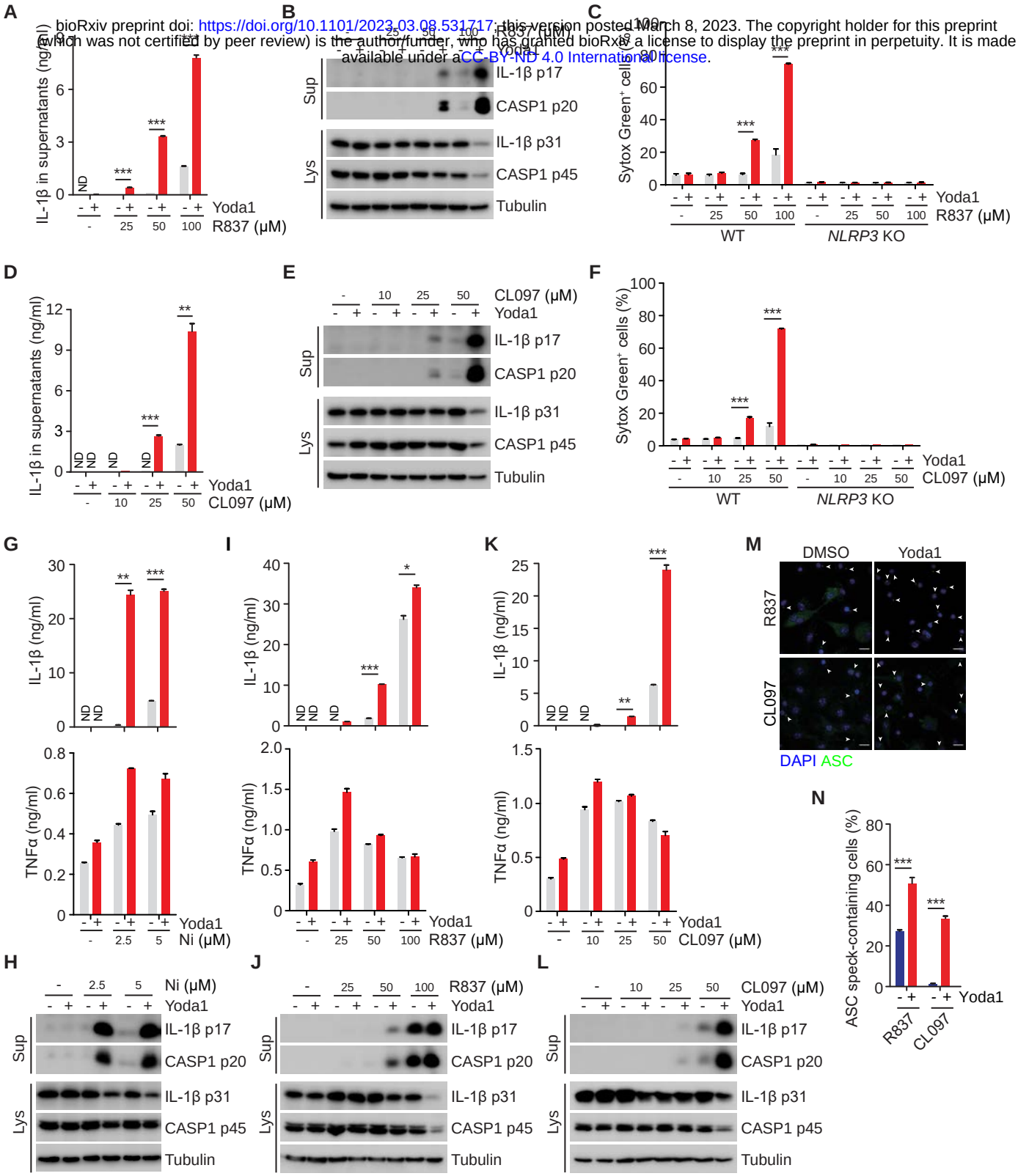

Fig. S1. The PIEZO1 agonist Yoda1 lowers the threshold of NLRP3 inflammasome activation. (**A**, **D**) ELISA measurements of IL-1β in culture supernatants from THP-1 primed with 1 μg/ml LPS for 3 h and followed by treatment with imiquimod R837 (**A**) or CL097 (**D**). (**B**, **E**) Immunoblotting of culture supernatants (Sup) and lysates (Lys) from LPS-primed THP-1 treated as in panel A and D. Antibodies againist IL-1β and Caspase-1 (CASP1) were used. Antibody against Tubulin was used as a loading control. (**C**, **F**) Uptake of Sytox Green in LPS-primed THP-1 WT and *NLRP3* KO cells treated as in panel A and D. (**G**, **I**, **K**) ELISA measurements of IL-1β and TNFα in culture supernatants from LPS-primed BMDMs treated with nigericin (Ni) (**G**), R837 (**I**), CL097 (**K**) as indicated in presence or absence of Yoda1 25 μM. (**H**, **J**, **L**) Immunoblotting of culture supernatants (Sup) and lysates (Lys) from LPS-primed BMDMs treated as in panel G, I, K. Antibodies againist IL-1β and Caspase-1 (CASP1) were used. Antibody against Tubulin was used as a loading control. (**M**) Representative immunofluorescence images of ASC speck formation in LPS-primed BMDMs stimulated with 50 μM R837 or 25 μM CL097 in the presence or absence of 25 μM Yoda1. White arrows indicate ASC specks. Scale bars: 10 μm. (**N**) Quantification of macrophages containing ASC specks in panel M. "ND" not detected. *$p < 0.05$, **$p < 0.01$, ***$p < 0.001$. Data are representative of at least three independent experiments.

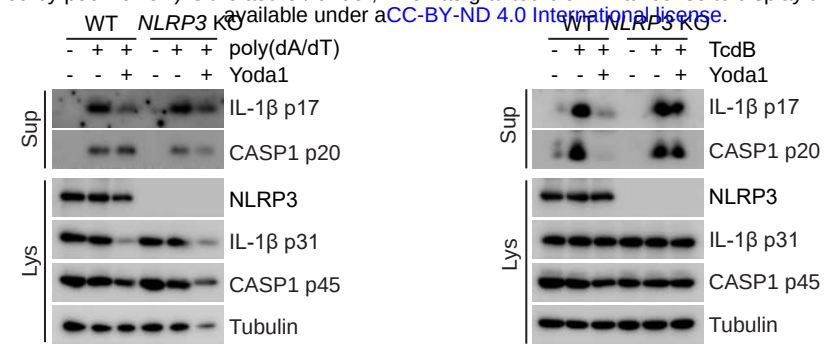

Fig. S2. Yoda1 don't show enhancing effects on AIM2- and NLRC4 inflammasome activation. (**A**, **B**) Immunoblotting of culture supernatants (Sup) and lysates (Lys) from LPS-primed WT and *NLRP3* KO BMDMs transfected with 1μg/ml poly(dA:dT) for 4 h (**A**) or treated with 1 nM TcdB for 2 h (**B**) in presence or absence of 25 μM Yoda1. Antibodies againist IL-1β and Caspase-1 (CASP1) were used. Antibody against Tubulin was used as a loading control. Data are representative of three independent experiments.

Fig. S3. Validation of *PIEZO1* KO, *PIEZO2* KO and *PIEZO1/2* dKO THP-1 cells. (**A**-**C**) Sequences of *PIEZO1* and/or *PIEZO2* alleles validated by Sanger sequencing in *PIEZO1* KO (**A**), *PIEZO2* KO (**B**), *PIEZO1/2* dKO (**C**). The sequences of sgRNAs are indicated by arrows. A mutation is highlighted in red, "-" indicates a deleted nucleotide, "..." in *PIEZO1* alleles indicates a fragment of 34 bps; "..." in *PIEZO2* alleles indicates a fragment of 96 bps. The seqeuncing was performed once.

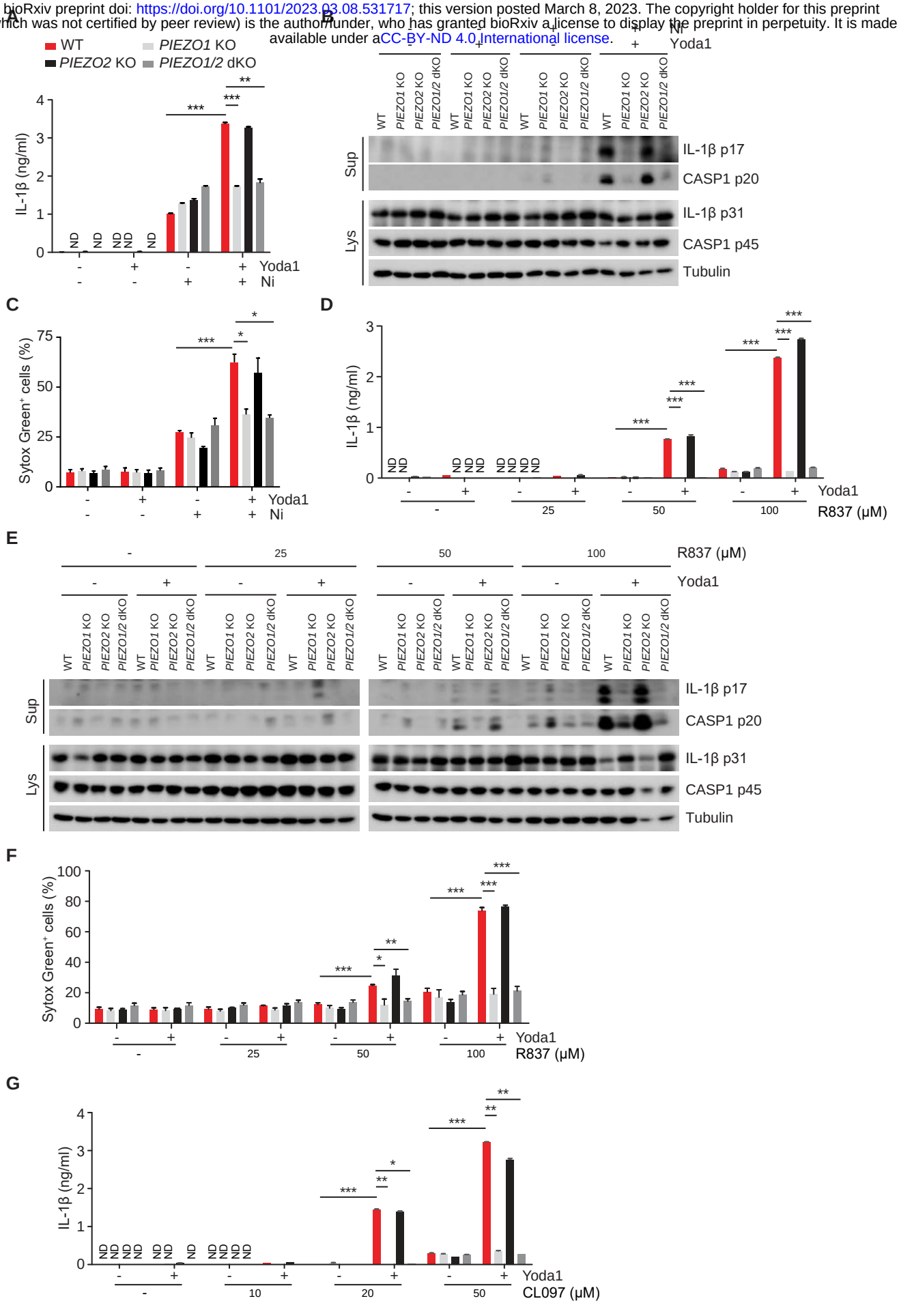

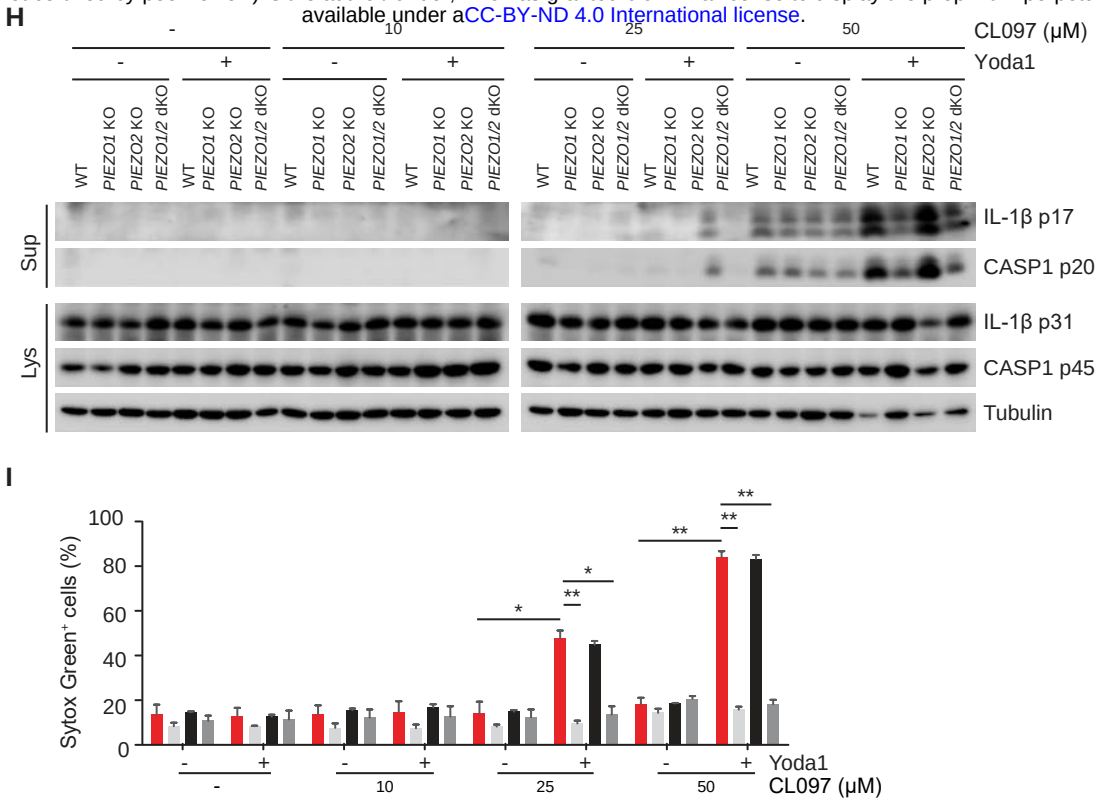

Fig. S4. Deleted of *PIEZO1* abolishes the sensitizing effect of Yoda1 on NLRP3 inflammasome activation. (**A**, **D**, **G**) ELISA measurements of IL-1β in culture supernatants in THP-1 wild type (WT), *PIEZO1* KO, *PIEZO2* KO and *PIEZO1/2* dKO cells primed with 1 μg/ml LPS for 3 h and followed by treatment with nigericin (**A**), R837 (**D**) and CL097 (**G**) as indicated in presence or absence of 25 μM Yoda1. (**B**, **E**, **H**) Immunoblotting of culture supernatants (Sup) and lysates (Lys) from LPS-primed cells in experiments as described in panel A, D and G. Antibodies againist IL-1β and Caspase-1 (CASP1) were used. Antibody against Tubulin was used as a loading control. (**C**, **F**, **I**) Uptake of Sytox Green from LPS-primed cells in experiments as described in panel A, D and G. Sytox Green uptake was analyzed by FACS after staining. "ND" not detected. **p* < *0.05*, ***p* < *0.01*, ****p* < *0.001*. Data are representative of at least three independent experiments.

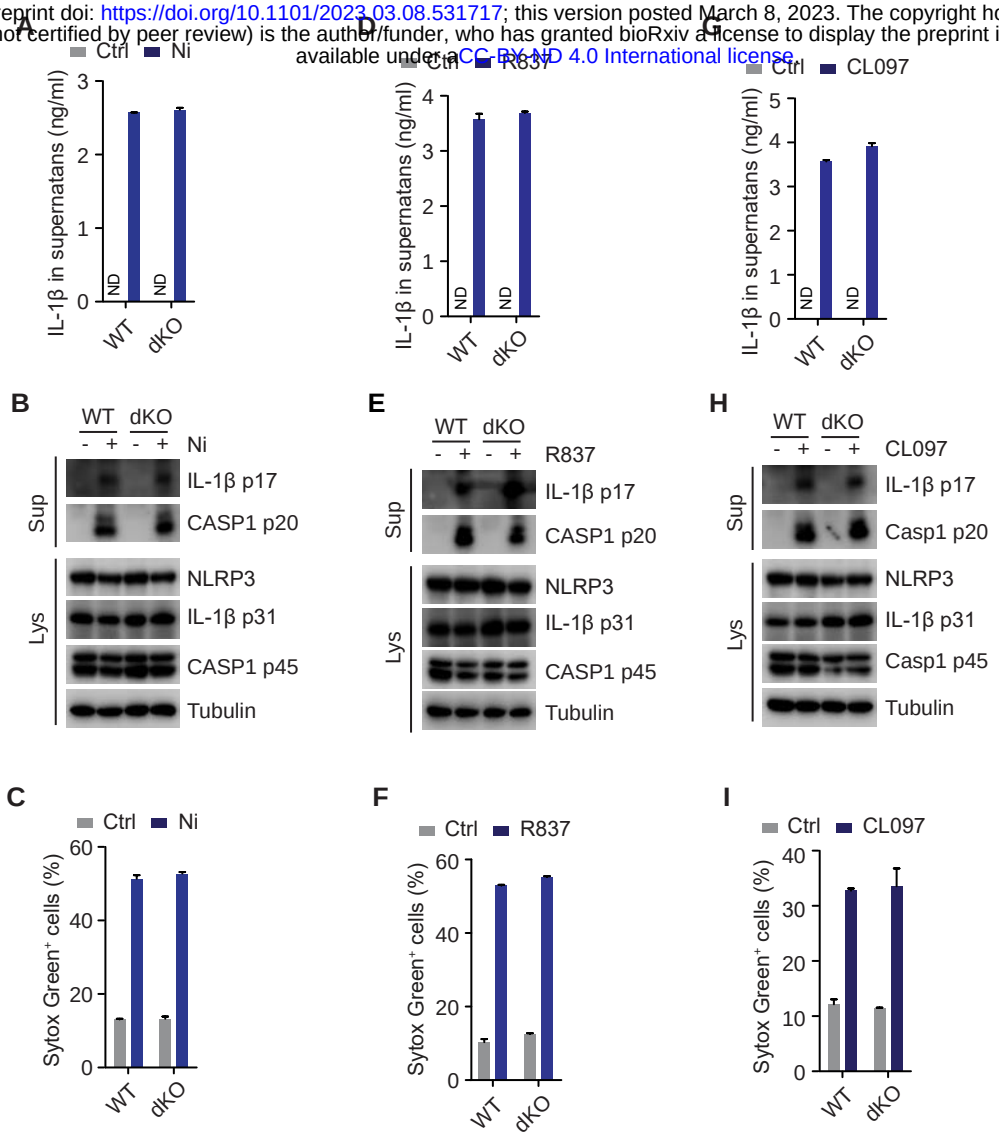

Fig. S5. PIEZO1 and PIEZO2 are not involoved in canonical NLRP3 inflammasome activation. (**A**, **D**, **G**) ELISA measurements of IL-1β in culture supernatants in THP-1 wild type (WT) and *PIEZO1/2* dKO (dKO) cells primed with 1 μg/ml LPS for 3 h and followed by treatment with 15 μM nigericin (Ni) (**A**), 150 μM R837 (**D**) and 75 μM CL097 (**G**). (**B**, **E**, **H**) Immunoblotting of culture supernatants (Sup) and lysates (Lys) from LPS-primed cells in experiments as described in panel A, D and G. Antibodies againist IL-1β and Caspase-1 (CASP1) were used. Antibody against Tubulin was used as a loading control. (**C**, **F**, **I**) Uptake of Sytox Green from LPS-primed cells treated as in panel A, D and G. Sytox Green uptake was analyzed by FACS after staining. Data are representative of three independent experiments. “ND” means not detected. Data are representative of at least three independent experiments.

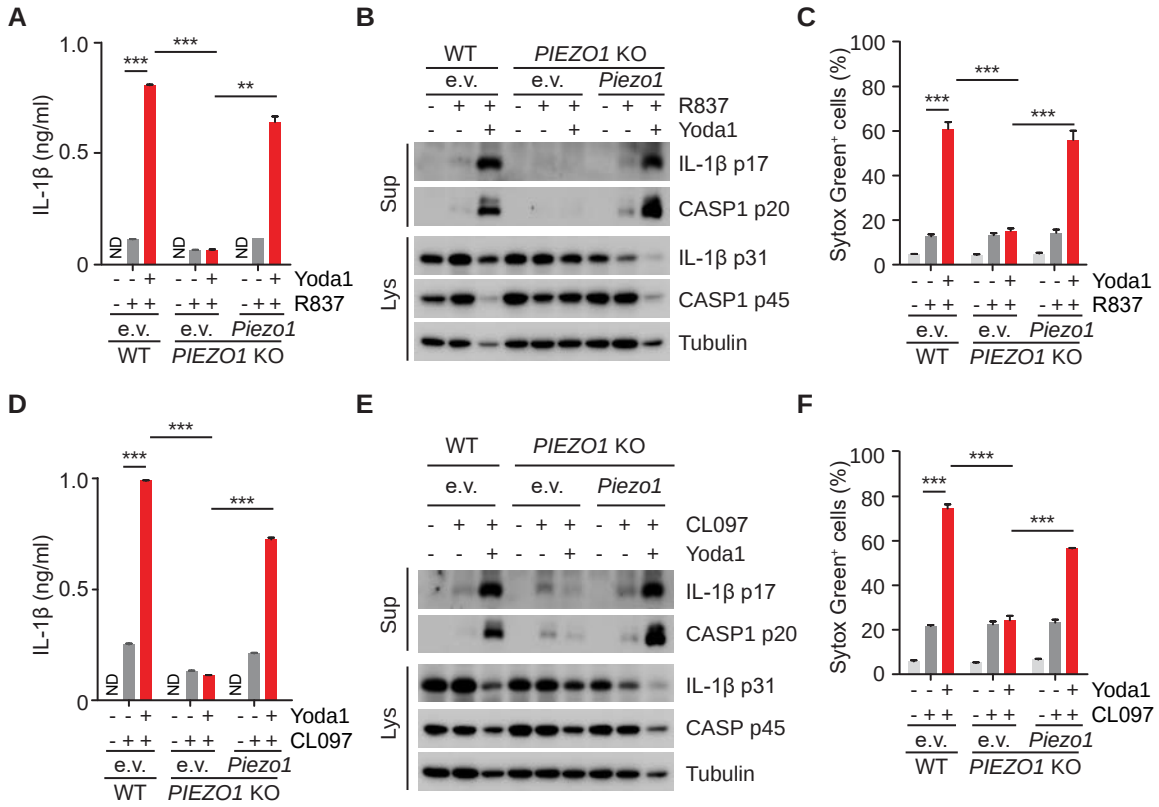

Fig. S6. Reconstitution of Piezo1 restores the sensitizing effect of Yoda1 on NLRP3 inflammasome activation in *PIEZO1* KO cells. (**A**, **D**) ELISA measurements of IL-1β in culture supernatants in WT and *PIEZO1* KO THP-1 cells expressing empty vector (e.v.) or mouse Piezo1. Cells were primed with 1 μg/ml LPS for 3 h, followed by treatment with 100 μM R837 (**A**), 50 μM CL097 (**D**) in presence or absence of 25 μM Yoda1. (**B**, **E**) Immunoblotting of culture supernatants (Sup) and lysates (Lys) from LPS-primed cells in experiments as described in panel A and D. Antibodies against IL-1β and Caspase-1 (CASP1) were used. Antibody against Tubulin was used as a loading control. (**C**, **F**) Uptake of Sytox Green from LPS-primed cells in experiments as described in panel A and D. Sytox Green uptake was analyzed by FACS after staining. "ND" not detected. $^{**}p < 0.01$, $^{***}p < 0.001$. Data are representative of at least three independent experiments.

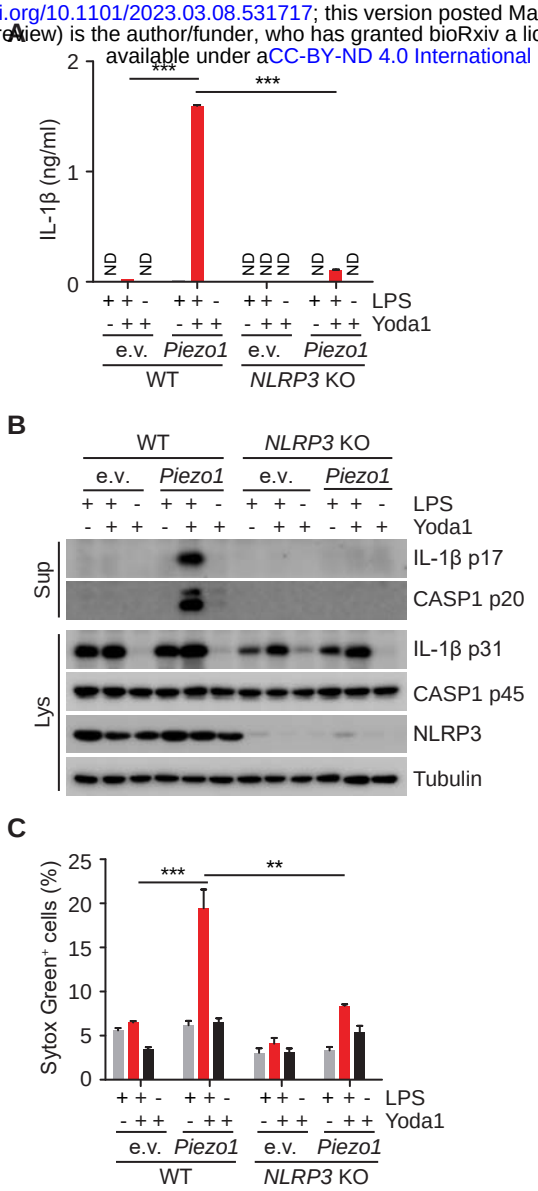

Fig. S7. Yoda1 alone is sufficient to activate NLRP3 inflammasome in cells ectopically-expressing Piezo1. (**A**) ELISA measurements of IL-1β in culture supernatants in WT and *NLRP3* KO THP-1 cells expressing empty vector (e.v.) or mouse Piezo1. Cells were primed with or without 1 μg/ml LPS for 3 h, followed by treatment with 25 μM Yoda1. (**B**) Immunoblotting of culture supernatants (Sup) and lysates (Lys) from cells in experiments as described in panel A. Antibodies against IL-1β and Caspase-1 (CASP1) were used. Antibody against Tubulin was used as a loading control. (**C**) Uptake of Sytox Green in cells in experiments as described in panel A. Sytox Green uptake was analyzed by FACS after staining. "ND" not detected. $^{**}p < 0.01$, $^{***}p < 0.001$. Data are representative of at least three independent experiments.

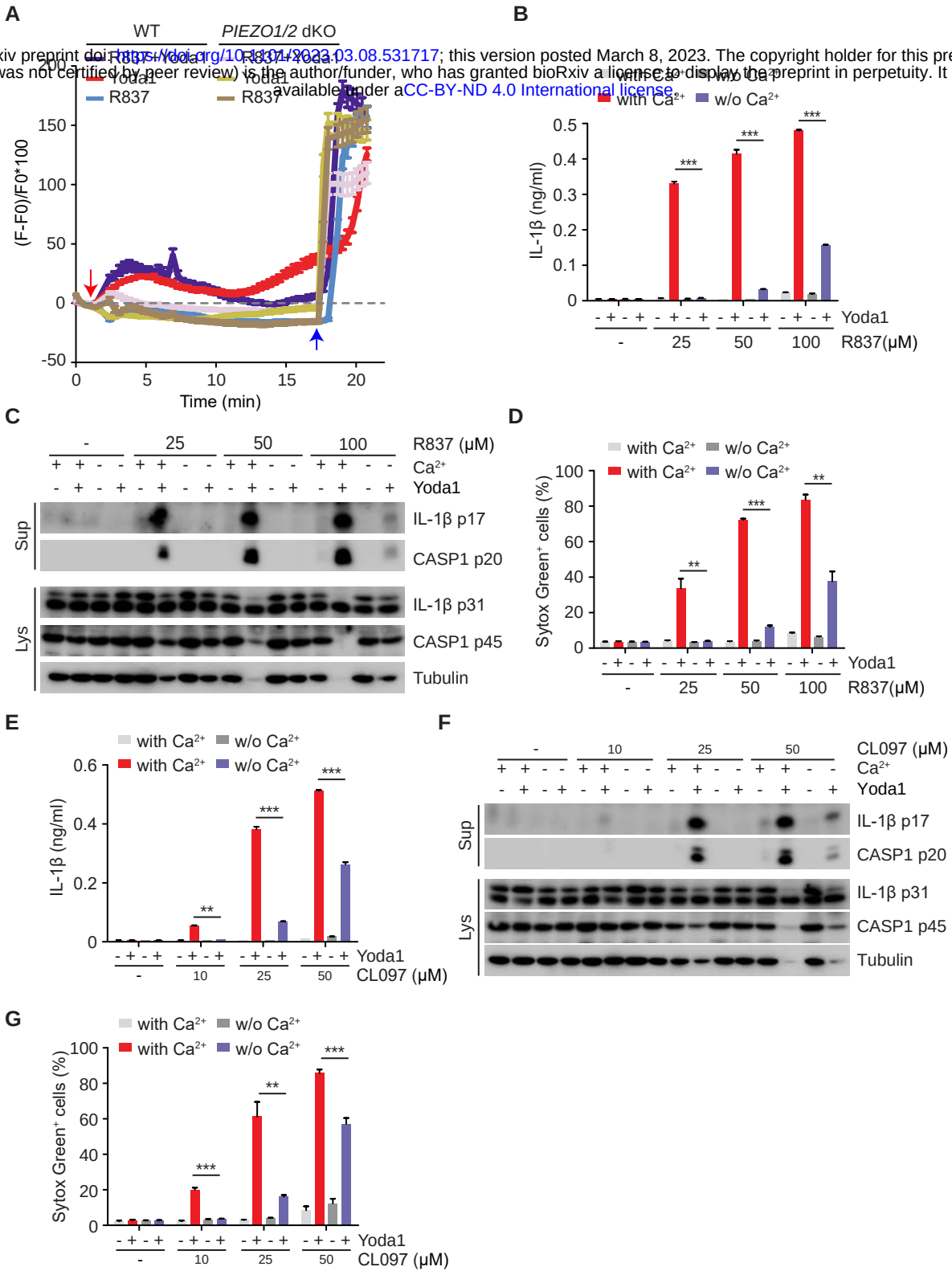

Fig. S8. Ca^{2+} influx is required for the enhaning effect of PIEZO-mediated mechanosensing on NLRP3 inflammasome activation. (**A**) Measurement of cytosolic Ca^{2+} levels in WT and *PIEZO1/2* dKO THP-1 cells using a Ca^{2+} reporter jGCaMP7s. Cells were treated with 100 μM R837, 25 μM Yoda1 or 100 μM R837 plus 25 μM Yoda1. The images were acquired using a Nikon spinning-disk microscope with an interval of 20s. Stimuli were added into the culture medium at 1 min as indicated by a red arrow, and ionomycin was added at end of the experiments as indicated by a blue arrow. Fluorescence intensities of individual cells over time were quantified. (**B**, **E**) ELISA measurements of IL-1β in culture supernatants from LPS-primed THP-1 treated with R837 (**B**), CL097 (**E**) as indicated in presence or absence of 25 μM Yoda1 in medium with Ca^{2+} or without (w/o) Ca^{2+}. (**C**, **F**) Immunoblotting of culture supernatants (Sup) and lysates (Lys) from LPS-primed THP-1 cells in experiments as described in panel B and E. Antibodies against IL-1β and Caspase-1 (CASP1) were used. An antibody against Tubulin was used as a loading control. (**D**, **G**) Uptake of Sytox Green in LPS-primed THP-1 cells in experiments as described in panel B and E. Sytox Green uptake was analyzed by FACS after staining. $^{**}p < 0.01$, $^{***}p < 0.001$. Data are representative of at least three independent experiments.

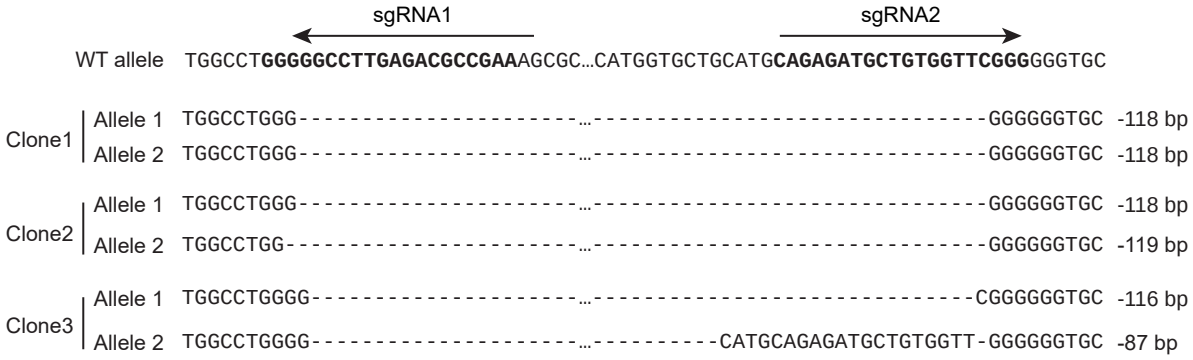

Fig. S9. Generation of THP-1 *KCNN4* KO cells using CRISPR/Cas9-mediated gene editing. Validation of *KCNN4* KO THP-1 cells by Sanger Sequencing. sgRNAs were indicated by arrows. "-" means a deleted nucleotide, "..." means a fragment of 65 bps.

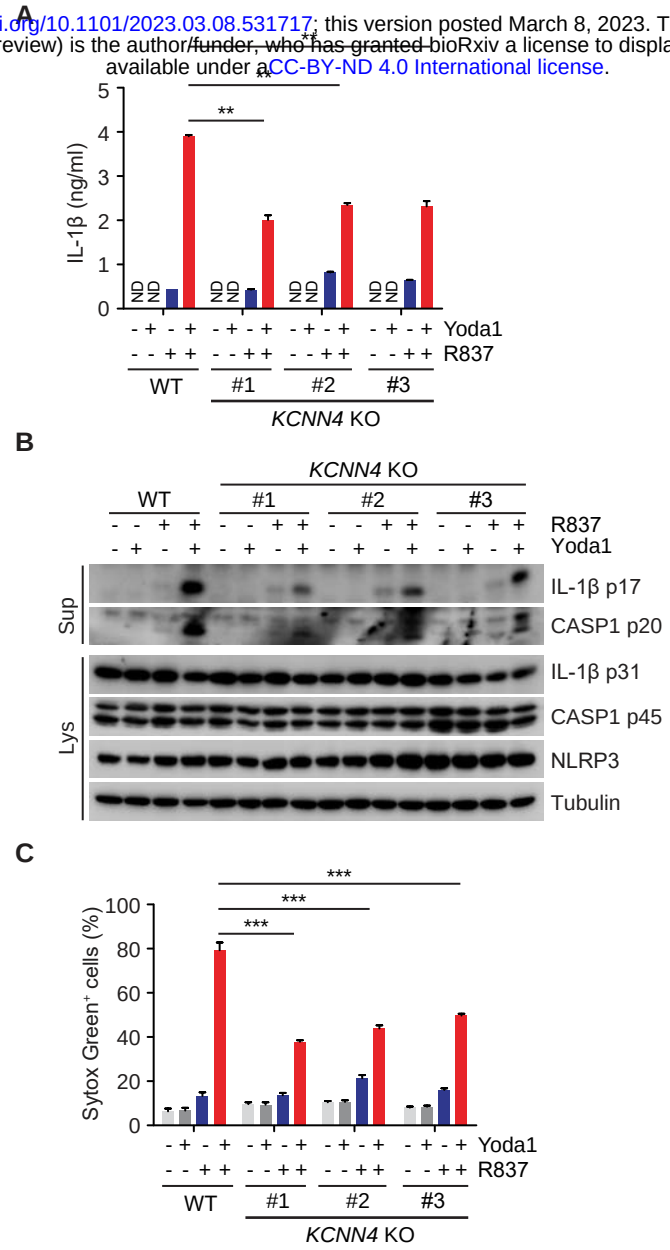

Fig. S10. Deletion of KCNN4 abolishes the sensitizing effect of Yoda1 on NLRP3 inflammasome activation. (**A**) ELISA measurements of IL-1β in culture supernatants from WT and *KCNN4* KO THP-1 cells primed with 1 µg/ml LPS for 3 h and followed by treatment with 100 µM R837 in presence or absence of 25 µM Yoda1 for 1.5 h. (**B**) Immunoblotting of culture supernatants (Sup) and lysates (Lys) from LPS-primed cells in experiments as described in panel A. Antibodies against IL-1β, Caspase-1 (CASP1) and NLRP3 were used. An antibody against Tubulin was used as a loading control. (**C**) Uptake of Sytox Green in LPS-primed cells in experiments as described in panel A. "ND" not detected. $^{**}p < 0.01$, $^{***}p < 0.001$. Data are representative of three independent experiments.

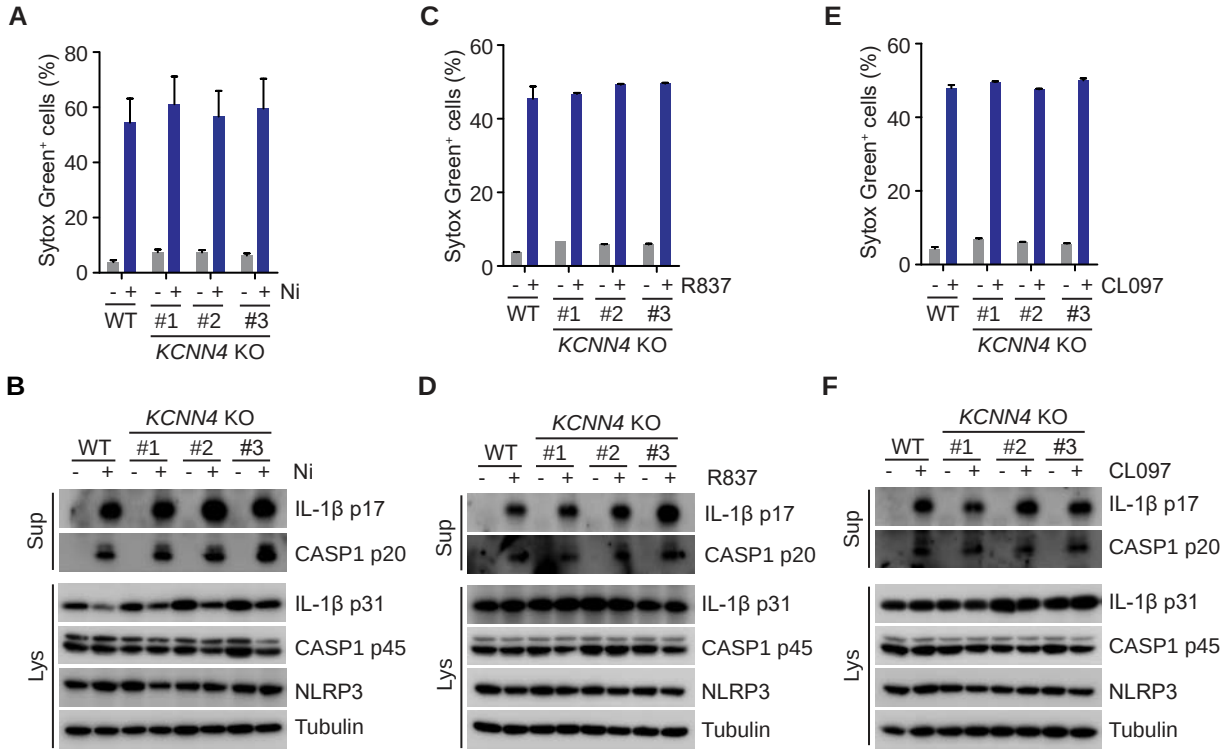

Fig. S11. KCNN4 is not involoved in canonical NLRP3 inflammasome activation. (**A**, **C**, **E**) Uptake of Sytox Green in WT and *KCNN4* KO THP-1 cells primed with1 µg/ml LPS for 3 h and followed by treatment with 15 µM nigericin for 1 h (**A**), 150 µM R837 for 1.5 h (**C**), 75 µM CL097 for 40 min (**E**). Sytox Green uptake was analyzed by FACS after staiing. (**B**, **D**, **F**) Immunoblotting of culture supernatants (Sup) and lysates (Lys) from LPS-primed cells in experiments as described in panel A, C and E. Antibodies against IL-1β, Caspase-1 (CASP1) and NLRP3 were used. An antibody against Tubulin was used as a loading control. Data are representative of three independent experiments.

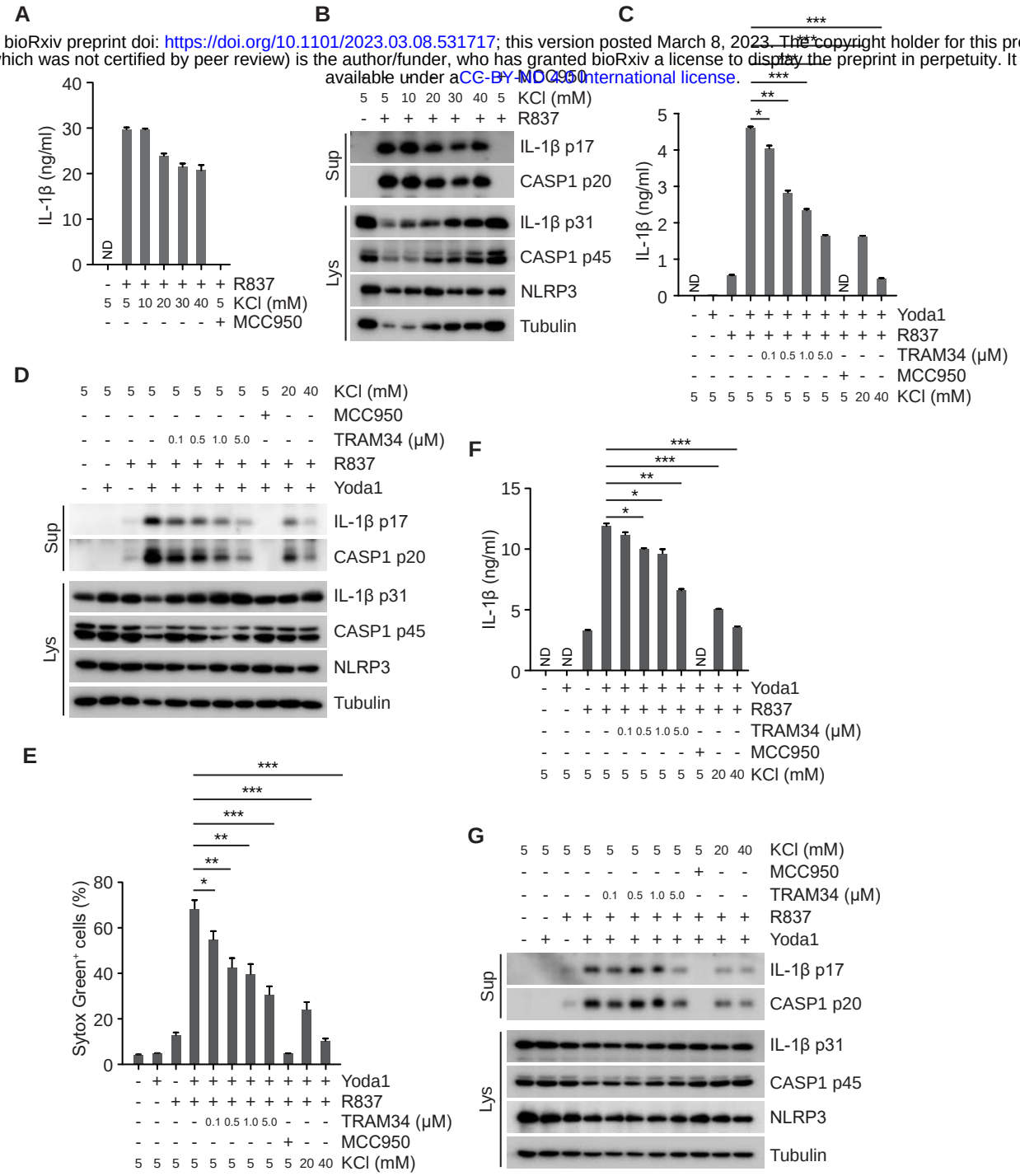

Fig. S12. Inhibition of KCNN4 blocks the effect of Yoda1 on NLRP3 inflammasome activation. (**A**) ELISA measurements of IL-1β in culture supernatants from LPS-primed BMDMs treated with 100 μM R837 in medium containing indicated concentration of extracellular KCl. (**B**) Immunoblotting of culture supernatants (Sup) and lysates (Lys) from LPS-primed BMDMs in experiments as described in panel A. Antibodies against IL-1β, Caspase-1 (CASP1) and NLRP3 were used. An antibody against Tubulin was used as a loading control. (**C**) ELISA measurements of IL-1β in culture supernatants from LPS-primed THP-1 cells treated with 100 μM R837, 25 μM Yoda1 or 100 μM R837 plus 25 μM Yoda1 in presence of TRAM34, 10 μM MCC950 or extracellular KCl as indicated for 1.5 h. (**D**) Immunoblotting of culture supernatants (Sup) and lysates (Lys) from THP-1 cells in experiments as described in panel C. (**E**) Uptake of Sytox Green in THP-1 cells in experiments as described in panel C. (**F**) ELISA measurements of IL-1β in culture supernatants from LPS-primed BMDMs treated with 50 μM R837, 25 μM Yoda1 or 50 μM R837 plus 25 μM Yoda1 in presence of TRAM34, 10 μM MCC950 or extracellular KCl as indicated for 1.5 h. (**G**) Immunoblotting of culture supernatants (Sup) and lysates (Lys) from LPS-primed BMDMs treated as in panel F. Antibodies against IL-1β, Caspase-1 (CASP1) and NLRP3 were used. An antibody against Tubulin was used as a loading control. “ND” not detected. *$p < 0.05$, **$p < 0.01$, ***$p < 0.001$. Data are representative of at least three independent experiments.

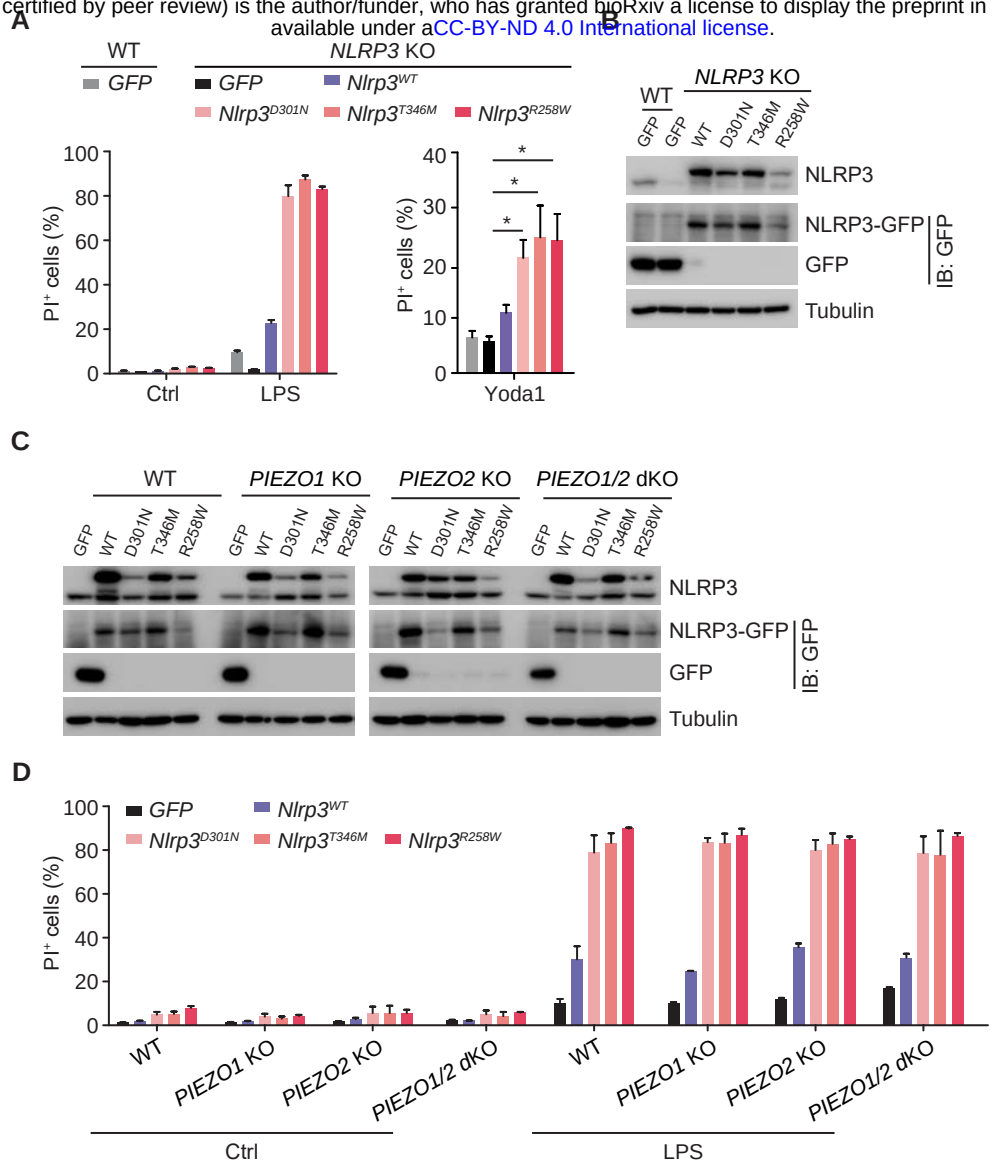

Fig. S13. Yoda1 is sufficient to activate NLRP3 inflammasome activation in cells expressing CAPS-causing NLRP3 mutants. (**A**) Uptake of Propidium Iodide (PI) in WT and *NLRP3* KO THP-1 cells expressing GFP, WT- or D301N-, T346M-, R258W mutated mouse Nlrp3. Cells were treated with vehicle,1 µg/ml LPS or 25 µM Yoda1. Propidium Iodide uptake was analyzed by FACS after staining. (**B**) Immunoblotting of lysates from WT and *NLRP3* KO THP-1 cells expressing GFP, WT- or D301N-, T346M-, R258W mutated Nlrp3 as decribed in panel A. Antibodies against NLRP3 and GFP were used. An antibody against Tubulin was used as a loading control. (**C**) Immunoblotting of lysates from WT, *PIEZO1* KO, *PIEZO2* KO and *PIEZO1/2* dKO THP-1 cells expressing GFP, WT- or D301N-, T346M-, R258W mutated Nlrp3. Antibodies against NLRP3 and GFP were used. An antibody against Tubulin was used as a loading control. (**D**) Uptake of Propidium Iodide (PI) in WT, *PIEZO1* KO, *PIEZO2* KO and *PIEZO1/2* dKO THP-1 cells expressing GFP, WT- or D301N-, T346M-, R258W mutated mouse Nlrp3. Cells were treated with vehicle or 1 µg/ml LPS for 6 h. Propidium Iodide uptake was analyzed by FACS after staining. *$p < 0.05$. Data are representative of at least three independent experiments.